

博士論文

論文題目 Trans-omic analysis reveals differences in

glucose-responsive regulation of liver

metabolism in obese *ob/ob* and wild-type mice

(野生型マウスと *ob/ob* 肥満マウスの肝代謝糖応答性
制御のトランスオミクス比較解析)

氏 名 小鍛治 俊也

Abstract

Glucose metabolism is homeostatically regulated by metabolic organs including the liver, and impaired glucose tolerance associated with obesity causes postprandial hyperglycemia, resulting in type 2 diabetes. Glucose metabolism is regulated by complex multi-omic network across metabolomic, transcriptomic and signaling molecule layers, denoted as “trans-omic” network. However, regulatory trans-omic network for glucose metabolism in the liver and its impairment in obesity remain unexplored. Here I constructed regulatory trans-omic networks for glucose-responsive metabolic reactions of the liver during oral glucose administration of wild type (WT) and leptin-deficient obese (*ob/ob*) mice by integrating multi-omic time course data based on information in several databases. In WT mice, metabolic reactions were globally regulated by rapid glucose-responsive metabolites as allosteric regulators and substrates, and by Akt-dependent glucose-responsive genes of metabolic enzymes in a time scale of 10 minutes. Especially, coenzymes, such as ATP and NADP⁺, played a central role in regulation of metabolic reactions. By contrast, in *ob/ob* mice, most of the rapid regulations of metabolic reactions by glucose-responsive metabolites was absent; instead, slowly changed glucose-responsive gene expression regulate metabolic reactions in a time scale of hours. The conserved regulations of metabolic reactions among both WT and *ob/ob* mice were quite limited. Thus, these trans-omic network analysis demonstrated that glucose-responsive metabolism in the liver is orchestrated by rapid allosteric and substrate regulations in the healthy state, and by slow transcriptional regulations in the obese state.

Table of Contents

1.	Introduction.....	6
	1.1 Essential function of liver in blood glucose homeostasis and its impairment in obesity	6
	1.2 Elucidation of regulatory system of metabolism through trans-omic analysis.....	6
5	1.3 Purpose of this study.....	7
2.	Materials and Methods.....	9
	2.1 Mouse studies.....	9
	2.2 Metabolomic analysis	9
	2.3 Lipidomic analysis	11
10	2.4 Glycogen content assay.....	11
	2.5 Triglyceride assay	12
	2.6 RNA sequencing	12
	2.7 qRT-PCR.....	13
	2.8 Western blotting.....	13
15	2.9 Identification of glucose-responsive molecules.....	15
	2.10 Identification of differences of the amounts of molecules at 0 min between WT mice and <i>ob/ob</i> mice.....	16
	2.11 Clustering analysis	16
	2.12 Pathway enrichment analysis.....	17
20	2.13 Prediction of transcription factor binding motif and inference of regulatory connections between TFs and genes	17
	2.14 Insulin signaling pathway	19

	2.15 Construction of regulatory trans-omic network of glucose-responsive metabolic reaction	19
	2.16 Determination of the values of K_m and K_i for metabolic enzymes	23
	2.17 Generation of a condensed trans-omic network based on metabolic pathway information	23
5		
	2.18 Implementation	24
	2.19 Data availability	24
	3. Results	25
	3.1 The pipeline of the construction of regulatory trans-omic network for glucose-responsive	
10	metabolic reactions	25
	3.2 Identification of glucose-responsive metabolites	28
	3.3 Identification of glucose-responsive genes and inference of regulatory connections	
	between TFs and genes	35
	3.4 Identification of glucose-responsive phosphorylation of insulin signaling molecules	44
15	3.5 The construction of regulatory trans-omic network for glucose-responsive metabolic	
	reactions	48
	3.6 Differences in the regulatory trans-omic networks between WT and <i>ob/ob</i> mice	53
	3.7 Differences in temporal control of the regulatory trans-omic network	59
	3.8 The regulatory trans-omic network for glucose-responsive metabolic reactions in	
20	carbohydrate metabolic pathway	63
	3.9 The regulatory trans-omic network for glucose-responsive metabolic reactions in lipid	
	metabolic pathway	64
	4. Discussion	73

	4.1 Regulatory trans-omic network for glucose-responsive metabolic reactions in WT and <i>ob/ob</i> mice.....	73
	4.2 Advantage of regulation of metabolic reaction by metabolite.....	74
	4.3 Obese-specific upregulation of pErk-mediated gene expression.....	74
5	4.4 Higher concentrations of carbohydrates in <i>ob/ob</i> mice	75
	4.5 Comparison with previous studies	75
	4.6 Future work.....	76
	5. References.....	78
	6. Acknowledgments.....	87

1. Introduction

1.1 Essential function of liver in blood glucose homeostasis and its impairment in obesity

Stability of blood glucose is indispensable for the maintenance of human life and health (1–3). Although a large amount of glucose flows into the body through several meals, change in organ-metabolism permits the maintenance of glucose homeostasis (4–6). Indeed, impairment of organ-metabolic regulation, commonly due to obesity and insulin resistance, results in hyperglycemia as shown in type 2 diabetes mellitus (4–6). The liver, into which dietary glucose flows directly through the portal vein, has primary function of the maintenance of glucose homeostasis (7, 8). Indeed, the liver is known as the only glucose-producing organ, which supplies glucose for extra-hepatic organs, and also as a glucose-utilizing organ, which disposes one third of orally administered glucose (8, 9). Oral intake of glucose produces drastic changes in the liver-metabolism, including not only glucose metabolism but also lipid and amino-acid metabolism, denoted here as glucose-responsive metabolism. However, global regulation of glucose-responsive metabolism in the liver and its impairment associated with obesity have yet to be identified.

1.2 Elucidation of regulatory system of metabolism through trans-omic analysis

Metabolism is a set of chemical reactions that convert from a metabolite to another. Chemical reactions in metabolism, denoted here as metabolic reactions, are regulated by metabolites and metabolic enzymes (Fig. 1). Regulation of metabolic reactions by metabolites consists of regulation by allosteric regulators and by substrates. An allosteric regulator refers to a metabolite that regulates metabolic enzyme activity. Regulation of metabolic reactions by metabolic enzymes consists of regulation by the amount of enzyme through gene expression, and regulation by enzyme activity through post-translational modifications, including phosphorylation. The amount and phosphorylation of metabolic enzymes are regulated by transcription factors and signal molecules, respectively. Therefore, metabolic reactions are regulated by an integrated network consisting of metabolites, gene expression and phosphorylation of metabolic enzymes, transcription factors, and signaling molecules. The regulatory mechanism of metabolic reactions in the liver and its impairment associated with obesity can be elucidated by the comprehensive and simultaneous measurements of

metabolites, gene expression and phosphorylation of metabolic enzymes, transcription factors, and signaling molecules, and their network integration.

Omic measurements, such as metabolomic, transcriptomic and proteomic measurements, allow us to comprehensively measure corresponding molecules in each omic layer, and simultaneous multi-omic measurements have recently been available (10–14). Trans-omic analysis has been proposed for the construction of global biochemical network using simultaneously measured multi-omic data based on direct molecular interaction, not indirect statistical relationship (15–17). An insulin-induced regulatory trans-omic network for metabolism of FAO hepatoma cells has been previously constructed by integration of the simultaneously measured multi-omic measurements, and found the selective regulation of the trans-omic network depending on doses of insulin (15, 18). However, the regulatory trans-omic network for glucose-responsive metabolic reactions of the liver, and its impairment associated with obesity have yet to be identified.

1.3 Purpose of this study

In this study, to reveal the global regulatory mechanism of glucose-responsive metabolism in the liver, and its impairment associated with obesity, I constructed the regulatory trans-omic networks for glucose-responsive metabolic reactions of the liver of wild type (WT) and leptin-deficient obese (*ob/ob*) mice (19). I administered glucose to mice orally, measured multi-omic data with my colleagues, and integrated into a trans-omic network. The *ob/ob* mice become profoundly obese by overeating due to deficiency of the anorexigenic hormone leptin, and have widely been used as a model mice for obesity and insulin resistance (19). In WT mice, glucose-responsive metabolic reactions were mainly regulated by the rapid response of metabolites as allosteric regulators and substrates, and by Akt-dependent gene expression of metabolic enzymes. By contrast, in *ob/ob* mice, most of rapid regulations by metabolites disappeared. Instead, *ob/ob*-specific slow gene expression alteration regulated metabolic reactions. Thus, I identified regulations of metabolic reactions in the liver of WT and *ob/ob* mice, and demonstrated that they are globally different between WT and *ob/ob* mice.

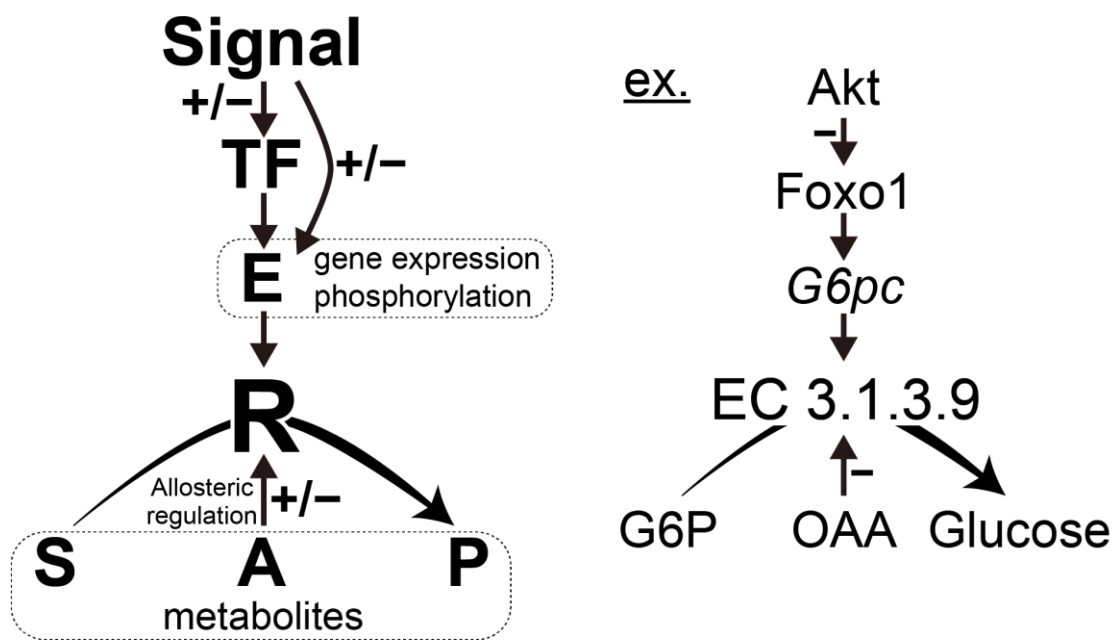


Figure 1. Regulatory network for metabolic reactions.

(Left) A generic metabolic reaction (R) is catalyzed by metabolic enzyme (E) and involves metabolites that function as the substrate (S), product (P), or allosteric regulator (A). For reversible reactions, the product is also a substrate and the substrate is also a product (not shown). Positive and negative signs indicate positive and negative regulation, respectively. Regulation of a metabolic reaction by a metabolic enzyme consists of regulation by changing the amount of enzyme through gene expression and regulation by changing enzyme activity through posttranslational modifications, in particular phosphorylation. Gene expression is regulated by one or more transcription factors (TFs) and signaling molecules (Signals) regulate both transcription factor activity and metabolic enzyme activity by changing phosphorylation status. (Right) The metabolic reaction EC 3.1.3.9 is regulated through changes in expression of the gene encoding glucose-6-phosphatase (G6pc) and changes in the abundance of the substrate glucose-6-phosphate (G6P) and the allosteric inhibitor oxaloacetate (OAA). Expression of the *G6pc* gene is stimulated by Forkhead box protein O1 (FoxO1), and the activity of FoxO1 is negatively regulated by Akt through phosphorylation.

2. Materials and Methods

2.1 Mouse studies

Mice experiments were approved by the animal ethics committee of The University of Tokyo. Ten-week-old male C57BL/6 wild-type and *ob/ob* mice were purchased from Japan SLC Inc. After overnight fasting (16 h), mice were administered 2 g/kg body weight of glucose or the same amount of water orally. Blood was collected from tail vein at the indicated times to measure blood glucose levels and insulin levels. At the end of the experiments, mice were sacrificed by cervical dislocation and the liver (whole or left lateral lobe) was dissected and immediately frozen in liquid nitrogen. The frozen liver was pulverized with dry ice to a fine powder with a blender and separated into tubes for each omic analysis (metabolomics, lipidomics, and transcriptomics), glycogen assay, triglyceride assay, Western blotting, and quantitative real-time polymerase chain reaction (qRT-PCR). For plasma metabolomic analysis, blood was collected from retro-orbital sinus into tubes containing 0.5 mg of EDTA soon after cervical dislocation and plasma was separated by centrifugation at $2,300 \times g$ for 15 min at 4°C.

2.2 Metabolomic analysis

Total metabolites and proteins were extracted from the liver with methanol:chloroform:water (2.5:2.5:1) extraction. Approximately 40 mg of the liver was suspended with 500 µL of ice-cold methanol containing internal standards [20 µM L-methionine sulfone (Wako), 2-Morpholinoethanesulfonic acid, monohydrate (Dojindo), and D-Camphor-10-sulfonic acid (Wako)] for normalization of peak intensities of mass spectrometry (MS) among runs, then with 500 µL of chloroform, and finally with 200 µL of water. After centrifugation at $4,600 \times g$ for 15 min at 4°C, the separated aqueous layer was filtered through a 5 kDa cutoff filter (Millipore) to remove protein contamination. The filtrate (320 µL) was lyophilized and, prior to MS analysis, dissolved in 50 µL water containing reference compounds [200 µM each of trimesate (Wako) and 3-aminopyrrolidine (Sigma-Aldrich)]. Proteins were precipitated by addition of 800 µL of ice-cold methanol to the interphase and organic layers and centrifuged at $12,000 \times g$ for 15 min at 4°C. The pellet was washed with 1 mL of ice-cold 80% (v/v) methanol and resuspended in 1 mL of sample buffer containing 1% SDS and 50

mM Tris-Cl pH8.8, followed by sonication. The total protein concentration was determined by bicinchoninic acid (BCA) assay and was used for normalization of metabolite concentration among samples.

Metabolites in plasma were extracted with methanol:chloroform:water (2.5:2.5:1). Plasma (40 μ L) was extracted with sequential addition of 400 μ L of ice-cold methanol containing the internal standards, 400 μ L of chloroform, and 120 μ L of water. After centrifugation at $10,000 \times g$ for 3 min at 4°C, the separated aqueous layer was filtered through a 5 kDa cutoff filter (Millipore) to remove protein contamination. The filtrate (300 μ L) was lyophilized and, prior to analysis by MS, dissolved in 50 μ L water containing the reference compounds.

All CE-MS experiments were performed using an Agilent 1600 Capillary Electrophoresis system (Agilent technologies), a G1603A Agilent CE-MS adapter kit, and a G1607A Agilent CE electrospray ionization (ESI)-MS sprayer kit by my research colleagues. Briefly, to analyze cationic compounds, a fused silica capillary [50 μ m internal Diameter (i.d.) \times 100 cm] was used with 1 M formic acid as the electrolyte (20). Methanol/water (50% v/v) containing 0.01 μ M hexakis(2,2-difluoroethoxy)phosphazene was delivered as the sheath liquid at 10 μ L/min. ESI-TOFMS was performed in positive ion mode, and the capillary voltage was set to 4 kV.

Automatic recalibration of each acquired spectrum was achieved using the masses of the reference standards ($[^{13}\text{C}$ isotopic ion of a protonated methanol dimer (2 MeOH+H)]⁺, m/z 66.0631) and ([hexakis(2,2-difluoroethoxy)phosphazene +H]⁺, m/z 622.0290). To identify metabolites, relative migration times of all peaks were calculated by normalization to the reference compound 3-aminopyrrolidine. The metabolites were identified by comparing their m/z values and relative migration times to the metabolite standards.

Quantification was performed by comparing peak areas to calibration curves generated using internal standardization techniques with methionine sulfone. The other conditions were identical to those described previously (21). To analyze anionic metabolites, a commercially available COSMO(+) (chemically coated with cationic polymer) capillary (50 μ m i.d. \times 105 cm) (Nacalai Tesque, Kyoto, Japan) was used with a 50 mM ammonium acetate solution (pH 8.5) as the electrolyte. Methanol/5 mM ammonium acetate (50% v/v) containing 0.01 μ M hexakis(2,2-difluoroethoxy)phosphazene was delivered as the sheath liquid at 10 μ L/min. ESI-TOFMS was performed in negative ion mode, and the capillary voltage was set to 3.5 kV. For anion

analysis, trimesate and D-Camphor-10-sulfonic acid were used as the reference and the internal standards, respectively. The other conditions were identical to those described previously (22). Agilent MassHunter software (Agilent technologies) was used for data analysis (21–23).

5 **2.3 Lipidomic analysis**

Total lipids were extracted from the liver by my research colleagues, as described previously (24, 25). Briefly, the frozen livers were suspended with methanol at a final concentration of 100 mg/mL of the weight of the liver. Chloroform (100 μ L) and methanol (100 μ L) containing internal standards [25 μ M deuterated (d3-) fatty acid (FA) (16:0), 25 μ M FA (18:0)-d3, 0.5 μ M Cer/Sph Mixture I (Avanti Polar Lipids), 5 μ M acylcarnitine (AC) (18:0)-d3, 5 μ M cholic acid-d4, 0.5 μ M phosphatidylglycerol 17:0/14:1, 0.5 μ M lysophosphatidylcholine (LPC) (17:0), 1 μ M triglyceride (24:0)- (8:0/8:0/8:0)-1,1,1-¹³C₃] were added to 100 μ L of the liver lipid mixture. After incubation for 1 h at room temperature, 20 μ L of water was added and the solution was mixed and incubated for 10 min at room temperature, followed by centrifugation at $2,000 \times g$ for 10 min at room temperature. The resulting supernatant was collected and injected into LC-MS systems (0.5 μ L for the positive ion mode, 1 μ L for the negative ion mode). LC–MS/MS analysis was performed using Triple TOF 5600+ System (SCIEX) with ACQUITY UPLC system (Waters) by my research colleagues. The reverse-phase LC separation was achieved by ACQUITY UPLC BEH column (particle size, 1.8 μ m, 50×2.1 mm i.d., Waters Corporation) at 45°C. The mobile phase was prepared by mixing solvents (A) acetonitrile/methanol/water (20/20/60; 5 mM ammonium acetate, 10 nM EDTA) and (B) isopropanol (5 mM ammonium acetate, 10 nM EDTA) at a flow rate of 300 μ L/min. Sixteen classes of lipids, each with different fatty acid composition, were analyzed, and each class was quantified by adding the area of species belonging to the class.

2.4 Glycogen content assay

Glycogen content was determined by my research colleagues, as previously described with some modifications (26). Approximately 20 mg of the liver was digested with 1.2 mL of 30% (w/v) potassium hydroxide solution for 1 h at 95°C and neutralized with 61.2 μ L of glacial acetic acid. The total protein concentration of the

liver digest was determined by BCA assay and adjusted to 1 μ g protein/ μ L. Glycogen was extracted from the liver digest with Bligh and Dyer method to remove lipids (27). The liver digest (50 μ L) was mixed with 120 μ L of ice-cold methanol, 50 μ L of chloroform, 10 μ L of 1% (w/v) linear polyacrylamide, and 70 μ L of water. After incubation on ice for 30 min, the mixture was centrifuged at $12,000 \times g$ to remove the separated aqueous layer. The glycogen was precipitated by addition of 200 μ L of methanol and centrifugation at $12,000 \times g$ for 30 min at 4°C, washed with ice-cold 80% (v/v) methanol and dried completely. The glycogen pellets were suspended in 20 μ L of 0.1 mg/mL amyloglucosidase (Sigma-Aldrich) in 50 mM sodium acetate buffer and incubated for 2 h at 55°C to digest glycogen. The concentration of the glucose produced from the glycogen was determined using the Amplex Red Glucose/Glucose Oxidase Assay kit glucose assay (Thermo Fisher Scientific), according to manufacturer's instruction.

2.5 Triglyceride assay

Triglyceride content was determined by my research colleagues. Total triglyceride was extracted with methanol:chloroform:water (2.5:2.5:1). Livers were suspended with methanol at final concentrations of 100 mg/mL (WT) or 25 mg/mL (*ob/ob*) of the weight of the liver. The suspension (800 μ L) was transferred into a new tube and mixed with chloroform (800 μ L) and water (320 μ L), followed by centrifugation at $4,600 \times g$ for 10 min at 4 °C. The organic phase (400 μ L) was collected into a new tube and resuspended in 20 μ L of Triton X-100. Samples were dried and resuspended in 180 μ L water. The concentration of triglyceride in the samples was determined using Triglyceride E test (Wako), according to the manufacturer's instruction.

2.6 RNA sequencing

The quantification of transcripts was performed by my research colleagues. Total RNA was extracted from the liver using RNeasy Mini Kit (QIAGEN) and QIAshredder (QIAGEN) and assessed for quantity using Nanodrop (Thermo Fisher Scientific) and for quality using the 2100 Bioanalyzer (Agilent Technologies). cDNA libraries were prepared using SureSelect strand-specific RNA library preparation kit (Agilent

Technologies). The resulting cDNAs were subjected to 100-bp paired-end sequencing on an Illumina HiSeq2500 Platform (Illumina) (28).

Sequences were aligned to the mouse reference genome obtained from Ensembl database (29, 30) (GRCm38/mm10, Ensembl release 70) using the software package TopHat (v.2.0.9) (31, 32), software in the Tuxedo tool. Cufflinks (v.2.2.1), software in the Tuxedo tool, was used to assemble transcript models from aligned sequences and to estimate the number of transcripts as an indication of gene expression (31, 32). The number of transcripts was shown as fragments per kilobase of exon per million mapped fragments (FPKM).

2.7 qRT-PCR

qRT-PCR was performed by my research colleagues, as previously described (33). Briefly, total RNA was extracted from the liver using RNeasy Mini Kit (QIAGEN) and QIAshredder (QIAGEN) and reverse-transcribed into complementary DNA (cDNA) using the High-Capacity RNA-to-cDNA Kit (Applied Biosystems), according to the manufacturer's instructions. The cDNA samples were amplified using Power SYBR Green PCR Master Mix (Applied Biosystems) and Step ONE plus Real-Time PCR system (Applied Biosystems), according to the manufacturer's protocols. The primer sequences used in the qRT-PCR analysis are listed in Table 1. The fold change was calculated using the mean expression of *Rpl4* and *Gusb* as reference.

2.8 Western blotting

Western blotting was performed by my research colleagues. Total proteins were extracted from the liver with methanol:chloroform:water (2.5:2.5:1) extraction. Ice-cold methanol was added to the liver at a concentration of 100 mg/mL of the weight of the liver, and the suspension (400 μ L) was mixed with chloroform (400 μ L) and water (160 μ L), followed by centrifugation at $4,600 \times g$ for 10 min at 4°C. The aqueous and organic phases were removed and 800 μ L of ice-cold methanol was added to the interphase to precipitate proteins. The resulting pellet was suspended with 400 μ L of lysis buffer [10 mM Tris-HCl (pH 6.8) in 1% SDS] and incubated for 15 min at 65°C, followed by sonication. The protein lysate was centrifuged $12,000 \times g$ for 3 min

Table 1. Primer sequences for RT-PCR.

Name	Pathway	Forward	Reverse
Acacb	Lipid synthesis	AGGTTCCAGATGCTAATGGGT	GCCCAGGATAAAGCTGGTCAT
Acat2	Cholesterol synthesis	CCCGTGGTCATCGTCTCAG	GGACAGGGCACCATTGAAGG
Acly	Glycolysis / gluconeogenesis	ACCCTTTCACCTGGGGATCACA	GACAGGGATCAGGATTCCTTG
Cyp51	Cholesterol synthesis	GACAGGAGGCAACTTGCTTTC	GTGGACTTTTCGCTCCAGC
Dhcr24	Cholesterol synthesis	TCATGATCAACCTGATGGACA	GGCTCCACTCGAACAATCTG
Dhcr7	Cholesterol synthesis	GCCAAGACACCACCTGTGACAG	TGGACGCCTCCCACATAACC
Ebp	Cholesterol synthesis	TGTCCTACAGCTTGTGGTGTCT	AATAAACGGGGTGGCCTATC
Fasn	Lipid synthesis	ATTGGTGGTGTGGACATGGTC	CCCAGCCTTCCATCTCCTG
Fdft1	Cholesterol synthesis	ATGGAGTTCGTCAAGTGTCTAGG	CGTGCCGTATGTCCCCATC
Fdps	Cholesterol synthesis	GGAGGTCCTAGAGTACAATGCC	AAGCCTGGAGCAGTTCTACAC
G6pc	Glycolysis / gluconeogenesis	GTGCAGCTGAACGTCTGTCTGTC	TCCGGAGGCTGGCATTGTA
Gapdh	Glycolysis / gluconeogenesis	AGGTCGGTGTGAACGGATTTG	TGTAGACCATGTAGTTGAGGTCA
Gck	Glycolysis / gluconeogenesis	ATGGCTGTGGATACTACAAGGA	TTCAGGCCACGGTCCATCT
Gpd1	Lipid synthesis	ATGGCTGGCAAGAAAGTCTG	CGTGCTGAGTGTTGATGATCT
Hmgcr	Cholesterol synthesis	AGCTTGCCCGAATTGTATGTG	TCTGTTGTGAACCATGTGACTTC
Hmgcs1	Cholesterol synthesis	AACTGGTGCAGAAATCTCTAGC	GGTTGAATAGCTCAGAACTAGCC
Hsd17b7	Cholesterol synthesis	GCTCACTGTGACACCGTACAA	CCGGTTTTTGGTGGAAGAG
Idi1	Cholesterol synthesis	GGTTCAGCTTCTAGCGGAGA	TCGCCTGGGTTACTTAATGG
Lpin1	Lipid synthesis	CTCCGCTCCCGAGAGAAAG	TCATGTGCAAATCCACGGACT
Lss	Cholesterol synthesis	TCGTGGGGGACCCTATAAAAC	CGTCCTCCGCTTGATAATAAGTC
Msmo1	Cholesterol synthesis	GCTGTGCAGTCATTGAGGACAC	GGGATGTGCGTATTCTGCTTCG
Mvd	Cholesterol synthesis	ATGGCCTCAGAAAAGCCTCAG	TGGTCGTTTTTAGCTGGTCCT
Mvk	Cholesterol synthesis	GGTGTGGTCGGAACCTCCC	CCTTGAGCGGGTTGGAGAC
Pklr	Glycolysis / gluconeogenesis	TCAAGGCAGGGATGAACATTG	CACGGGTCTGTAGCTGAGTG
Pmvk	Cholesterol synthesis	AAAATCCGGGAAGGACTTCGT	AGAGCACAGATGTTACCTCCA
Sc5d	Cholesterol synthesis	CCTTAATGAAACACCCACAGTTT	CTCCAGCAGGAACAGTGAGAC
Gusb	Control	GGCTGGTGACCTACTGGATTT	GGCACTGGGAACCTGAAGT
Rpl4	Control	CCGTCCCCTCATATCGGTGTA	GCATAGGGCTGTCTGTTGTTTTT

at 4°C to remove debris. The total protein concentration of the resulting supernatant was determined by BCA assay. Antibodies were purchased from Cell Signaling Technology, as follows: pIrβ (Tyr1150/Tyr1151) (#3024), total Irs1 (#2382), pErk1/2 (Thr202/Tyr204) (#9101), phosphorylated cAMP responsive element binding protein (pCreb) (Ser133) (#9198), phosphorylated eukaryotic translation initiation factor 4e (peif4e) (Ser209) (#9741), pAkt (Ser473) (#9271), pS6 (Ser235/Ser236) (#2211), pGsk3β (Ser9) (#9336), pGs (Ser641) (#3891), pFoxO1 (Ser256) (#9461), and β-Actin (#4967). Antibodies against total Irβ (sc-711) and β-Actin (sc-47778) were from Santa Cruz Biotechnology, and pIrs1 (Tyr612) (09-432), total Irs2 (MABS15) were from Millipore. pGp (Ser15) was made in house as previously described (26). The proteins (2 μg or 10 μg) were separated on SDS-PAGE and blotted with the antibodies. Immunodetection was performed using Immobilon Western Chemiluminescent HRP Substrate (Millipore) or SuperSignal West Pico PLUS Chemiluminescent Substrate (Thermo Fisher Scientific), and the Western blot signals were detected using a luminoimage analyzer (LAS-4000; Fujifilm or ChemiDoc Touch MP; Bio-Rad) and quantified with the TotalLab TL120 analysis software (Nonlinear Dynamics). β-Actin was used as a loading control.

2.9 Identification of glucose-responsive molecules

Molecules that were detected in less than half of replicates in either WT mice or *ob/ob* mice at any time point after oral glucose administration were removed from the analysis. A molecule with a statistically significant change in response to oral glucose administration was defined as a glucose-responsive molecule according to the following criteria. The fold change of the mean amount at each time point over the mean amount at fasting state (0 min) was calculated for each molecule. The significance of the change at each time point was tested by two-tailed Welch's *t*-test for each metabolite, and by CuffDiff (v. 2.2.1), software in the Tuxedo tool (31, 34), for each gene. Metabolites and genes that showed an absolute log₂ fold change larger than 0.585 ($2^{0.585} = 1.5$) and an FDR-adjusted p value (q value) less than 0.1 at any time point were defined as glucose responsive metabolites (Fig. 4) and genes (Fig. 7). The q values were calculated by Storey's procedure (35). For Western blotting data, proteins that showed an absolute log₂ fold change larger than 0.585 at any time point, except for 240 min of WT mice, were defined as glucose-responsive (Fig. 10). Because of the small number of WT mice

at 240 min ($n = 1$), I did not use the fold changes at the time point. To define an increase or decrease in time courses with changes in both directions at different times, I used the direction of change compared to time 0 at the earliest time point that showed a significant change. Metabolites that responded to oral water administration were determined by the same procedure as the identification of glucose-responsive metabolites.

5

2.10 Identification of differences of the amounts of molecules at 0 min between WT mice and *ob/ob* mice

The differences of the amounts of molecules between WT mice and *ob/ob* mice before glucose administration (0 min) were determined by fold change and statistical test using the following procedure. The fold change of the mean amount of *ob/ob* mice at 0 min over the mean amount of WT mice at 0 min was calculated for each molecule. The significance of differences were tested by two-tailed Welch's *t*-test for each metabolite and phosphorylation, and by CuffDiff (v. 2.2.1) (31, 34) for each gene expression. Molecules that showed an absolute \log_2 fold change larger than 0.585 ($2^{0.585} = 1.5$) and a *q* value less than 0.1 were defined as different molecules in amount between WT mice and *ob/ob* mice. The *q* values were calculated by Storey's procedure for polar metabolite and gene expression (35). The *q* values were calculated by Benjamini–Hochberg procedure for lipid and phosphorylation (36), because of the small numbers of molecules.

2.11 Clustering analysis

Time courses for the expression of each gene of WT mice and *ob/ob* mice were normalized by subtracting the average of the expression values of time courses of both mice and then dividing the resulting values by the standard deviation (Z-score normalization). I combined the 2 time courses of WT and *ob/ob* mice for each gene and performed hierarchical clustering of the combined time courses using Euclidean distance and Ward's method (Fig. 9). The genes with significant differences between WT mice and *ob/ob* mice at any time point (*q* value < 0.1) or a significant response at any time point either in WT mice or *ob/ob* mice (*q* value < 0.1) were selected for the clustering analysis (7845 genes). For the selection, *p* value was calculated by CuffDiff (v. 2.2.1) (31, 34), and *q* value was calculated by Storey's procedure (35).

2.12 Pathway enrichment analysis

I performed pathway enrichment analysis of glucose-responsive genes (Table 4), genes showing the differences in the amounts of expression between WT mice and *ob/ob* mice before oral glucose administration (Table 3), and the genes in each cluster (Fig. 9). The enrichment of the genes in each pathway was determined using one-tailed Fisher's exact test. I used the genes detected in more than half of the replicates in WT mice and *ob/ob* mice at all time points as a background. In pathway enrichment analysis of the glucose-responsive genes, I used the pathways in Metabolism, Genetic Information Processing, and Cellular Processes from the KEGG database (37, 38). I used the same pathways in enrichment analysis of the genes showing the differences in the amounts of expression between WT mice and *ob/ob* mice before oral glucose administration. In pathway enrichment analysis of the genes in each cluster, I used pathways in Metabolism and Genetic Information Processing from the KEGG database (37, 38). I also used the KEGG pathway "cholesterol metabolism", which included terpenoid backbone biosynthesis (mmu00900) and steroid biosynthesis (mmu00100).

2.13 Prediction of transcription factor binding motif and inference of regulatory connections between TFs and genes

The flanking regions around the major transcription start site of genes were extracted from GRCm38/mm10 (Ensembl, release 71) using Ensembl BioMart (39). The region from -300 bp to +100 bp of the major transcription start site was defined as the flanking region, according to the FANTOM5 analysis of time course (40). The transcription factor binding motifs in each flanking region (Fig. 9B) were predicted using TRANSFAC Pro, a transcription factor database, and Match, a transcription factor binding motifs prediction tool (41, 42). The threshold for each transcription factor binding motif prediction was set using extended vertebrate_non_redundant_min_FP.prf, a parameter set in TRANSFAC Pro. Because some of the transcription factors known to regulate the metabolism of liver (43) are not included in this parameter set, I extracted the transcription factor binding motifs of PPARA, PPARG, FOXO1, and CHREBP1 from minFP_good.prf, and appended these transcription factor binding motifs and their parameters to

vertebrate_non_redundant_min_FP.prf. If a transcription factor has multiple binding motifs, I selected the binding motif that was based on the largest number of sequences.

For the inference of regulatory connections between TFs and genes, I performed transcription factor motif enrichment analysis of the genes in each cluster (Fig. 9B). The enrichment of transcription factor binding motif in the flanking regions of genes in each cluster was determined by one-tailed Fisher's exact test, and transcription factor binding motifs with q value less than 0.1 were defined as significantly enriched. The q values were calculated by Benjamini–Hochberg procedure (36). I used the genes analyzed in the hierarchical clustering as a background. To reduce the number of statistical tests, the clusters that contain 100 genes or more were analyzed. If a transcription factor binding motifs were enriched in the promoter regions of the genes in a cluster, I inferred the regulatory connections between the corresponding transcription factor and the genes in the cluster. To avoid overestimation, I examined the enrichment of transcription factor binding motif in two children clusters of a cluster, and excluded the parent cluster from the inference if the transcription factor binding motif was significantly enriched in one of the two children clusters. The enrichment of transcription factor binding motif in the flanking regions of genes in each of two children clusters was determined by one-tailed Fisher's exact test, and transcription factor binding motifs with p value less than 0.01 were defined as significantly enriched. I used the genes in the parent cluster as a background.

For the validation of the inferred regulatory connections, I examined the overlap between the inferred genes of each transcription factor and those predicted from experimental ChIP data from the ChIP-Atlas database (44) (Fig. 9C). The genes for which ChIP-seq peaks of a transcription factor were detected in the flanking region around the transcription start sites were obtained using “Target genes,” a prediction tool in ChIP-Atlas. I used the flanking regions from -1000 bp to +1000 bp of the transcription start sites in Target Genes. The overlap between the inferred genes and genes from ChIP data was determined by one-tailed Fisher's exact test, and those with p value less than 0.01 were defined as significant.

2.14 Insulin signaling pathway

Insulin signaling pathway in Fig. 10 is a subset of the nodes of the insulin signaling pathway in the KEGG database (mmu04910) (37, 38) with regulatory input to cAMP responsive element binding protein (Creb) from the PI3K-Akt signaling pathway (mmu04151) and MAPK signaling pathway (mmu04010) in the KEGG database.

2.15 Construction of regulatory trans-omic network of glucose-responsive metabolic reaction

The regulatory trans-omic networks for glucose-responsive metabolic reactions consisted of five layers—Insulin signal, TF, Enzyme, Reaction, and Metabolite—with inter- and intra-layer regulatory connections (Fig. 12). The Insulin signal layer is the insulin signaling pathway constructed in a previous phosphoproteomic study (18). I included in the Insulin signal layer signaling molecules that I analyzed by Western blotting for abundance or phosphorylation state or both; I did not include transcription factors, such as Foxo1, or metabolic enzymes, such as Gs, in this layer. The TF layer consisted of all transcription factors with the inferred regulatory connection (Fig. 9). The Enzyme layer consisted of all metabolic enzymes in the pathways in Metabolism obtained from the KEGG database (37, 38). The Reaction layer consisted of the metabolic reactions (based on EC number) corresponding to the metabolic enzymes in the Enzyme layer. The Metabolite layer consisted of all metabolites analyzed by CE-MS. Only the molecules and reactions corresponding to the genes that were expressed in at least one sample were included in the Insulin signal, TF, Enzyme, and Reaction layers. Not all 14,292 genes were included in the network.

Each layer included the corresponding glucose-responsive molecules. The Insulin signal layer involved signaling molecules showing glucose-responsive phosphorylation (Fig. 10). The TF layer included “glucose-responsive transcription factors,” which were defined as the transcription factors encoded by glucose-responsive genes or those showing glucose-responsive phosphorylation (Figs. 7 and 10). To avoid overestimation, the transcription factors with downstream genes that were not enriched in glucose-responsive upregulated genes or downregulated genes were excluded from glucose-responsive transcription factors. I used

the inferred regulatory connections for the identification of upstream of glucose-responsive genes (Fig. 9). The enrichment of the downstream genes in glucose-responsive genes was determined by one-tailed Fisher's exact test, and an enrichment with a q value less than 0.1 was defined as significant. The q values were calculated by Benjamini–Hochberg procedure (36).

5 The Enzyme layer included “glucose-responsive metabolic enzymes,” which were defined as the metabolic enzymes encoded by glucose-responsive genes or those showing glucose-responsive phosphorylation (Figs. 7 and 10). The Reaction layer included “glucose-responsive metabolic reactions,” which were defined as metabolic reactions regulated by the glucose-responsive metabolites or the glucose-responsive metabolic enzymes or both. The Metabolite layer included the glucose-responsive metabolites (Fig. 4). I also determined
10 the direction of glucose-responsiveness, increase or decrease. To determine a direction for time courses with both increased and decreased time points, I used the direction of change at the earliest time point with a significant difference from time 0 (fasting state). I did not determine a direction (increase or decrease) for metabolic reactions, because I did not measure metabolic reaction activity.

To determine inter-layer and intra-layer regulatory connections, I used a process I have used previously (37,
15 38, 45). To determine regulatory connections from the Enzyme and Metabolite layers to Reaction layer, both the target of the regulatory connection (a metabolic reaction) and the regulating molecule (enzyme or metabolite) had to be glucose responsive. Among the Insulin signal, TF, and Enzyme layers, the inter-layer regulatory connections and intra-layer regulatory connections were determined using the directions of glucose-responsiveness of the regulating molecule and the regulated molecules, and the types of the inter-layer and
20 intra-layer regulatory connections, which were either designated positive or negative. I defined the positive inter-layer and intra-layer regulatory connections when both the regulating molecule and regulated molecule showed the same direction of change, that is both increased or both decreased. I defined the negative inter-layer and intra-layer regulatory connections when the regulating molecule and regulated molecule showed responses in the opposite direction, that is one increased and the other decreased.

25 The inter-layer regulatory connections from the Insulin signal layer to the TF layer and the Enzyme layer and the intra-layer regulatory connections in the Insulin signal layer mediated by phosphorylation were

determined based on the kinase-substrate relationship in the insulin signaling pathway constructed in a previous phosphoproteomic study (18). The insulin signaling pathway is a pathway comprise of several signaling pathways in the KEGG database (37, 38). The inter-layer regulatory connections from the TF layer to the Enzyme layer and the intra-layer regulatory connections in the TF layer were determined based on the relationship between transcription factors and gene expression inferred from transcription factor binding motif enrichment analysis. The types of the regulatory connections made by glucose-responsive transcription factors were defined according to the Gene Ontology Annotations obtained from the Mouse Genome Database (46) (Table 2). The transcription factors that were included in the list of DNA-binding transcription repressor (GO:0001227) and not in the list of DNA-binding transcription activator (GO:0001228) were defined as the transcription repressors. Foxo1 was added to the list of transcription activator based on the previous studies of gluconeogenesis (47, 48). The effects of the phosphorylation of transcription factors on the types of regulatory connections were defined according to the KEGG database (37, 38). The inter-layer regulatory connections from the Enzyme layer to the Reaction layer were determined by regulation of metabolic reactions by the corresponding metabolic enzymes according to the KEGG database (37, 38). The inter-layer regulatory connections from the Metabolite layer to the Reaction layer were of two types: regulation by allosteric regulator and regulation by the reaction's substrate or product. Allosteric regulatory connections were determined by allosteric regulation of metabolic reactions by metabolites according to the BRENDA database (45). I used the allosteric regulation reported for mammals (*Bos taurus*, *Felis catus*, *Homo sapiens*, "Macaca," "Mammalia," "Monkey," *Mus booduga*, *Mus musculus*, *Rattus norvegicus*, *Rattus rattus*, *Rattus sp.*, *Sus scrofa*, "dolphin," and "hamster"). Substrate and product regulatory connections were determined by regulation of metabolic reaction by its substrate or product according to the KEGG database (37, 38). Because the reversibility of metabolic reactions was not determined, metabolic reactions were assumed to be regulated by both the substrate and product.

In the comparison of the trans-omic networks between WT mice and *ob/ob* mice, I identified 4 types of regulatory connections; WT mice-specific, *ob/ob* mice-specific, common, and opposite regulatory connections. The regulatory connections were defined as WT mice-specific or *ob/ob* mice-specific if the connections were

Table 2. The types of the regulatory connections made by transcription factors

TF		
Activation	BBX	HOMEZ
	BEN	ING4
	CHCH	IRF1
	COE1	MAZR
	CPBP	MAZ
	CREB1	NFAT1
	CREBP1	P53
	CTCF	RELA
	DRI1	RNF96
	EGR1	SP100
	ERALPHA	SP1
	FOXO1	SREBP
	FREAC3	TATA
	GKLF	XBP1
	HIF1A	ZFP161
	HMG1Y	ZFX
Repression	DEAF1	
	HBP1	
	HES1	
	HIC1	
	POU6F1	

identified only in WT mice or *ob/ob* mice, as common if the connections were identified in both WT mice and *ob/ob* mice and the regulating molecules were common glucose-responsive molecules, as opposite if the connections were identified in both WT mice and *ob/ob* mice and the regulating molecules showed opposite responses.

5

2.16 Determination of the values of K_m and K_i for metabolic enzymes

I extracted K_m values of a substrate for metabolic enzyme, and K_i value of a metabolite for metabolic enzyme from *Mus musculus* and *Homo sapiens* from the BRENDA database (45) (Fig. 13). The values for mutant enzymes were excluded. I used the values for *Mus musculus* unless they were not available, then I used the values for *Homo sapiens*. When multiple values for the same enzyme and metabolite were present, I used their geometric mean. To compare with the metabolomic data, I changed the unit of the metabolomic data using the weight of protein per volume in the mouse liver (0.2 mg/L) (51, 52).

10

2.17 Generation of a condensed trans-omic network based on metabolic pathway

15 information

I condensed the regulatory trans-omic networks according to the following procedures (Fig. 14). First, I grouped the related metabolic reactions in a specific metabolic pathway into one “metabolic pathway node,” according to the KEGG metabolic map (37, 38). Second, I selected metabolic pathway nodes that exhibited significant associations with any glucose-responsive metabolites or transcription factors and created a “Pathway” layer with the nodes and their regulatory connections. I then classified the metabolic pathway nodes into 3 classes —carbohydrate, lipid, and amino acid— according to the KEGG database (37, 38). The association between the metabolic reactions in a metabolic pathway and those regulated by a glucose-responsive molecule was determined by one-tailed Fisher’s exact test, and associations with a p value less than 0.05 were defined as significant. I also selected glucose-responsive metabolites that exhibited significant associations with any metabolic pathway nodes. Third, I reduced the inter-layer regulatory connections from the Metabolite layer to the Pathway layer by removing the inter-layer regulatory connections that regulated

20

25

fewer than five metabolic reactions. I connected *Egr1* to pErk as an indirect downstream transcription factor on the previous observation (49, 50) (dashed arrow).

2.18 Implementation

- 5 Statistical tests, clustering analysis, enrichment analysis, and trans-omic network analysis were done using MATLAB 2017a (The Mathworks Inc.). Visualization of trans-omic network in Graph Modeling Language (GML) formats was done using Python 2.7 and VANTED (53).

2.19 Data availability

- 10 Sequencing data measured in this study have been deposited in the DNA Data Bank of Japan Sequence Read Archive (DRA) (www.ddbj.nig.ac.jp/) under the accession no. DRA008416. All of other omic data and the result of omic analysis are available with the article in pre-print server (54).

3. Results

3.1 The pipeline of the construction of regulatory trans-omic network for glucose-responsive metabolic reactions

In this study, I constructed the regulatory trans-omic networks for glucose-responsive metabolic reactions in the liver of WT and *ob/ob* mice, and I examined differences in global regulation of glucose-responsive metabolic reactions between WT and *ob/ob* mice (Fig. 2). Metabolic reactions are regulated by an integrated network consisting of (i) metabolites as allosteric regulators, substrates, and products, (ii) metabolic enzymes and their encoding genes, (iii) transcription factors, and (iv) signal molecules (Fig. 1). In this study, metabolites, gene expression, and signaling molecules were measured using multi-omic analyses, enzymatic assays, and Western blotting in the liver and blood of WT and *ob/ob* mice following oral glucose administration. I integrated these data with bioinformatic resources to construct regulatory trans-omic networks for glucose-responsive metabolic reactions of the liver in WT and *ob/ob* mice (Fig. 2).

WT and *ob/ob* mice were administered with glucose, and sacrificed at 0, 20, 60, 120, 240 min after administration, and the liver and blood were collected (Fig. 3A). With my research colleagues, I performed metabolomics, transcriptomics, and western blotting for the phosphorylation of insulin signaling molecules in the liver, and metabolomics in the blood (Fig. 3B). The liver samples provided data for signaling molecules, transcription factors, and enzymes involved in insulin signaling (Western blotting data), the gene expression of transcription factors and enzymes (transcriptomic data), and metabolites (metabolomic data). I identified molecules statistically changed by oral glucose administration, defined as glucose-responsive molecules (Figs. 4 to 11). Metabolites and genes that showed an absolute \log_2 fold change larger than 0.585 ($2^{0.585} = 1.5$) and an FDR-adjusted p value (q value) less than 0.1 at any time point compared to the fasting state (0 min) were defined as glucose-responsive. I also identified the differences in the amounts of molecules in the fasting state (0 min) between WT mice and *ob/ob* mice, but the information was not used to construct the networks in order to focus on “glucose-responsiveness”.

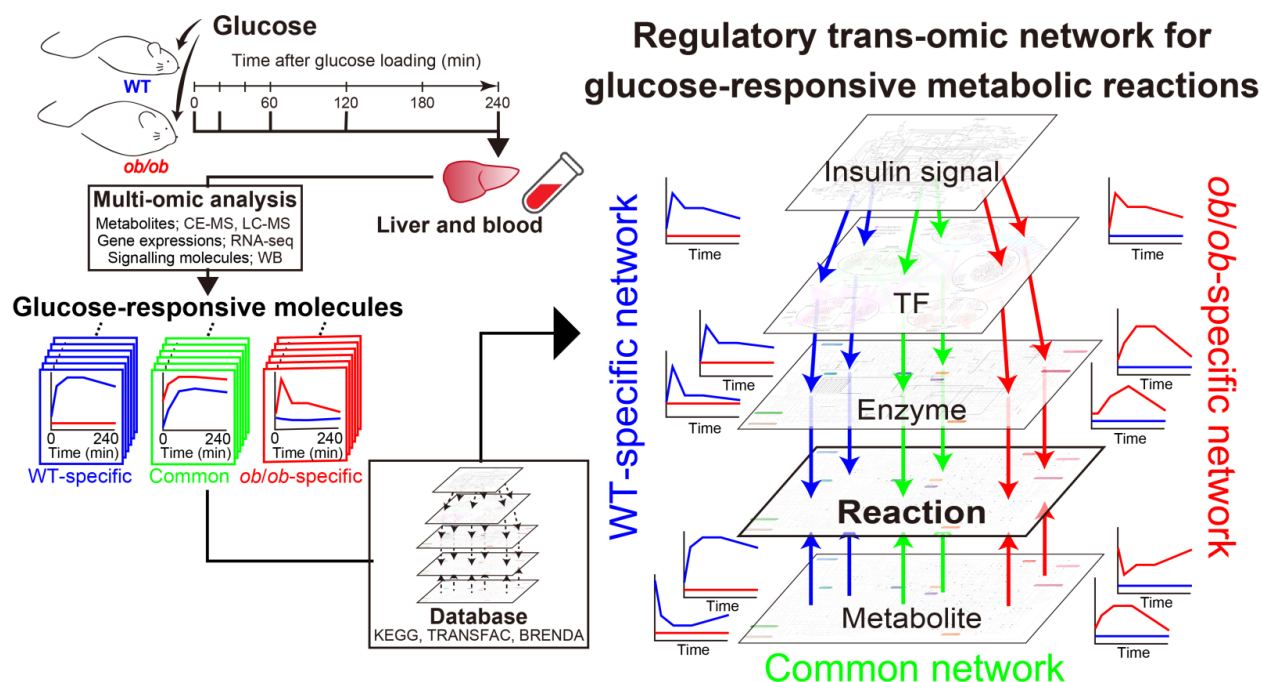


Figure 2. The pipeline of the construction of regulatory trans-omic network for glucose-responsive metabolic reactions.

I measured the time courses of multi-omic data from the liver and blood of WT mice and *ob/ob* mice following oral glucose administration and identified molecules that changed by oral glucose administration, which I defined as glucose-responsive molecules in each layer (see Materials and Methods: Identification of glucose-responsive molecules). I added inter-layer regulatory connections between glucose-responsive molecules in different layers using bioinformatic methods and information in public databases. The result was a regulatory trans-omic network for glucose-responsive metabolic reactions in the liver of WT and *ob/ob* mice. I identified regulatory trans-omic subnetworks specific to WT mice (blue), *ob/ob* mice (red), and common to both mice (green).

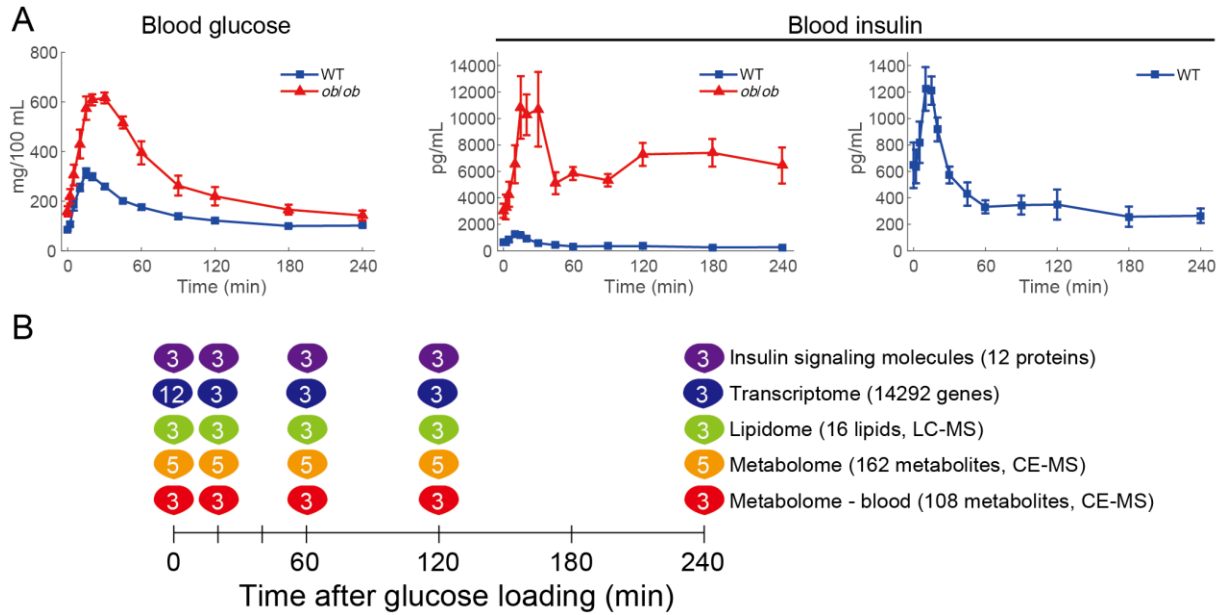


Figure 3. Oral glucose administration and multi-omic measurements.

(A) Blood glucose and blood insulin of WT mice (blue) and *ob/ob* mice (red) during oral glucose administration. The means and SEMs of 5 mice are shown. (B) I orally administered glucose to 16 h-fasting WT and *ob/ob* mice, and collected the liver and blood at 0, 20, 60, 120, 240 min after administration. I performed metabolomics, transcriptomics, and western blotting for the phosphorylation of insulin signal molecules in the liver, and metabolomics in the blood. The number of the mice in each measurement is shown at each time point.

I integrated the glucose-responsive molecules across multi-omic layers, and constructed the regulatory trans-omic networks for glucose-responsive metabolic reactions of the liver of WT and *ob/ob* mice (Fig. 12). The regulatory trans-omic network consisted of layers of insulin signaling molecules (Insulin signal), transcription factors (TF), the gene expression and phosphorylation of metabolic enzyme (Enzyme), metabolic reactions (Reaction), metabolites (Metabolite), and the regulatory links between the layers (Fig. 2). By comparing the regulatory trans-omic networks, I identified WT-specific elements, *ob/ob*-specific elements, and common elements in the glucose-responsive liver metabolic networks, denoted as common network, WT-specific network, and *ob/ob*-specific network, respectively.

3.2 Identification of glucose-responsive metabolites

Metabolomic changes in the liver of WT and *ob/ob* mice following oral glucose administration were measured using capillary electrophoresis mass spectrometry (CE-MS) and liquid chromatography mass spectrometry (LC-MS) (Figs. 4 and 5). 161 polar metabolites were quantified by CE-MS, including carbohydrates, amino acids and nucleic acids, and 15 lipids by LC-MS. Glycogen, a polar metabolite, and triglyceride, a lipid, were measured by enzymatic assays. I identified glucose-responsive metabolites in the liver of WT and *ob/ob* mice that showed statistically significant changes after oral glucose administration (Fig. 4). I also analyzed metabolites in mice administered with water, and found that no metabolites exhibited responses, except for isethionate in *ob/ob* mice, indicating that the glucose-responsive metabolites identified in this study are indeed “glucose-responsive”.

Of the 162 polar metabolites, I determined that the number of metabolites increased or decreased in both WT and *ob/ob* mice was limited: 7 increased in both WT and *ob/ob* mice and 8 metabolites decreased (Fig. 4B). Glucose-6-phosphate (G6P), the product of first step of glycolysis, increased in both WT and *ob/ob* mice (Fig. 4C). Note that, despite the difference in amounts between WT and *ob/ob* mice, G6P was identified as a glucose-responsive metabolite in both mice. Metabolites commonly decreased in both mice included the amino acids isoleucine (Ile), leucine (Leu), valine (Val), the nucleotide sugar UDP-glucose and 3-hydroxybutyrate (3-OH-butyrate), a ketone body (Fig. 4C). Although Leu had the significantly increased and decreased time points

in both mice, it was categorized as a decreased metabolite because the decreased time point was earlier than the increased time point (see Method).

Metabolomic analysis showed that the number of WT mice-specific glucose-responsive metabolites (42 = 23 increased + 19 decreased) was larger than *ob/ob* mice-specific glucose-responsive metabolites (24 = 18 increased + 6 decreased). Metabolites that increased only in WT mice included ATP; metabolites that decreased only in WT mice included NADP⁺ (Fig. 4C). Because ATP and NADP⁺ are involved in about 200 and 100 metabolic reactions, these cofactors are notable WT-specific glucose-responsive metabolites. This result suggested that many glucose-responsive metabolic reactions were regulated by ATP and NADP⁺ in WT mice and that the lack of glucose responsiveness in these two cofactors in *ob/ob* mice could produce a large difference in the regulatory mechanisms between the healthy and obese states. Of the 16 lipids, no lipids showed significant changes after oral glucose administration (Fig. 5).

Some metabolites are regulated not only in the liver but also in the blood through systemic circulation, contributing to glucose homeostasis. (e.g. the Cori cycle (lactate) and the glucose-alanine cycle) (55–57). Therefore, the time courses of 108 metabolites in the blood of WT and *ob/ob* mice following oral glucose administration were measured using CE-MS, and compared with the time courses of the metabolites in the liver (Fig. 6). In both WT and *ob/ob* mice, branched chain amino acids (BCAAs) and 3-OH-butyrate showed positive correlations between liver and blood (Fig. 6C). The decrease of these metabolite in the blood is consistent with the responses in human blood after oral glucose administration (58). Because the activity of branched-chain aminotransferase (Bcat) is much lower in the liver than in the muscle, the decrease of BCAAs in the liver may be indirectly regulated through the blood (59). In contrast, because ketone bodies are mainly produced in the liver (60), the decrease of the ketone body 3-OH-butyrate in the blood might reflect the regulation of ketogenesis in the liver. Note that these highly correlated metabolites were not identified as glucose-responsive metabolites in the blood of WT and *ob/ob* mice, possibly because of the small number of mice for metabolomic analysis of blood.

I also identified the significant differences of the amounts of metabolites in the liver between WT mice and *ob/ob* mice (Table 3). 46 metabolites showed higher abundances in *ob/ob* mice than in WT mice, including

(A) Left: The heat map of the time courses of 162 metabolites from the liver of WT and *ob/ob* mice following oral glucose administration. To investigate the changes from fasting state, two time courses of each metabolite were divided by the geometric mean of the values of WT mice and *ob/ob* mice in fasting state (0 min), and then log₂-transformed. Metabolites were ordered by hierarchical clustering using Euclidean distance and Ward's method. Right: The bars in the heat map are colored according to the glucose-responsiveness, meaning the change from fasting state (0 min), in the WT and *ob/ob* mice. Metabolites that showed an absolute log₂ fold change larger than 0.585 ($2^{0.585} = 1.5$) and an FDR-adjusted p value (q value) less than 0.1 at any time point were defined as glucose-responsive: increased (orange), decreased (purple), or were unchanged (white). To define an increase or decrease in time courses with changes in both directions at different times, I used the direction of change compared to time 0 at the earliest time point that showed a significant change. Metabolites written in red text indicate glucose-responsive metabolites specific to WT; blue text, specific to *ob/ob* mice; green text, common to both; pink text, opposite responses between WT mice and *ob/ob* mice; black text, no response to glucose. (B) Increased, decreased, and unchanged metabolites in the liver of WT mice and *ob/ob* mice: blue text, WT specific; red text, *ob/ob* specific; green text, glucose-responsive metabolites common to both; pink text, opposite responses between WT mice and *ob/ob* mice. The number of each type of glucose-responsive metabolites and their percentages out of the total quantified metabolites are shown. (C) Graphs showing the metabolites with responses that were common to both WT and *ob/ob* (green boxes), specific to WT mice (blue boxes), and specific to *ob/ob* mice (red boxes), and the metabolites that change in opposite directions in WT and *ob/ob* mice (pink boxes). Within the graphs, blue lines are the responses of the WT mice and red lines are the responses of the *ob/ob* mice. Data are shown as the mean and SEM of 5 mice.

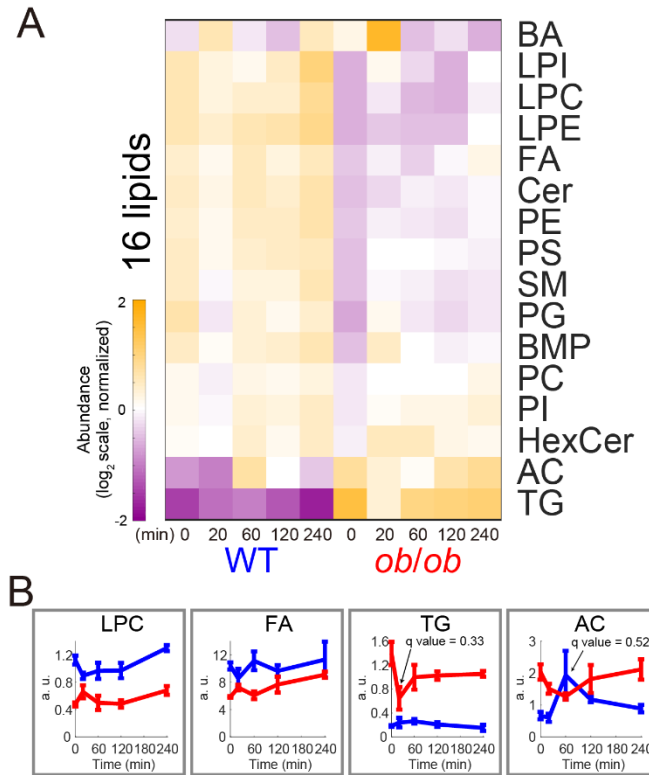


Figure 5. Time courses of lipidomic data in the liver.

(A) The heat map of the time courses of 16 lipids in the livers of WT and *ob/ob* mice during oral glucose administration. Two time courses of each metabolite were divided by the geometric mean of the values of WT mice and *ob/ob* mice in fasting state (0 min), and then log₂-transformed. Lipids were ordered by hierarchical clustering using Euclidean distance and Ward's method. No lipids showed significant change from fasting state (0 min) by oral glucose administration. (B) Time courses of the indicated lipids in the liver of WT mice (blue) and *ob/ob* mice (red) during oral glucose administration. Data are shown as the mean and SEM of 3 mice.

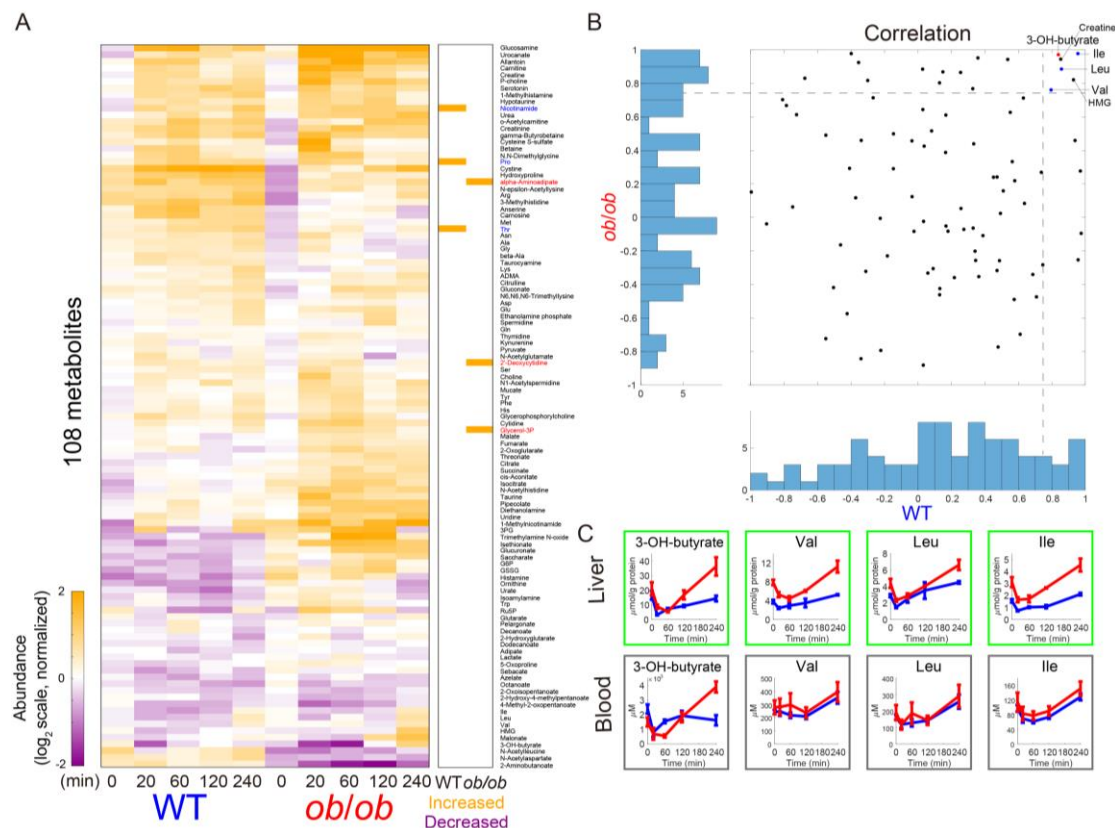


Figure 6. Time courses of metabolites in the blood.

(A) Left: The heat map of the time courses of 108 metabolites in the blood of WT and *ob/ob* mice following oral glucose administration. Two time courses of each metabolite were divided by the geometric mean of the values of WT mice and *ob/ob* mice in fasting state (0 min), and then log₂-transformed. Metabolites were ordered by hierarchical clustering using Euclidean distance and Ward's method. Right: The increased metabolites (orange) and unchanged metabolites (white) in WT mice and *ob/ob* mice. The changes from fasting state were determined by fold change and statistical test. (B) Histograms and scatter plot of Pearson's correlation coefficients between the time courses of metabolites measured in liver and blood in WT mice and *ob/ob* mice. Dashed lines correspond to correlation coefficients equal to 0.75. (C) Time courses of the indicated metabolites in the liver and blood of WT mice (blue) and *ob/ob* mice (red) following oral glucose administration. The indicated metabolites showed high correlations (correlation coefficient > 0.75) between the liver and the blood in both WT and *ob/ob* mice. The means and SEMs of mice are shown (n = 5 for liver, n = 3 for blood). The colors of the frames indicate common glucose-responsive metabolites (green).

Table 3. Metabolites showing the differences in the amounts between WT mice and ob/ob mice before oral glucose administration.

	Larger in <i>ob/ob</i> mice		Larger in WT mice
Polar metabolite	ATP	Adenosine	SAH
	UDP	Gluconate	Gly
	SAM+	Homoserine	PAP
	GTP	dGTP	Ornithine
	GSH	Spermidine	beta-Ala
	Gln	6-Phosphogluconate	Choline
	PEP	F1,6P	GMP
	UTP	Urate	Sarcosine
	Trp	Guanosine	Citrulline
	F6P	Ile	Saccharopine
	G6P	Pipecolate	Hypotaurine
	G1P	5-Aminovalerate	Betaine
	CDP	Cytidine	Tartrate
	Leu	N1-Acetylspermidine	Hydroxyproline
	GSSG	2PG	N,N-Dimethylglycine
	Isoamylamine	Pterin	2-Aminobutanoate
	Adenine	Mucate	Guanidinosuccinate
	Asn	γ-Guanidinobutyrate	Argininosuccinate
	Citrate	1-Methylnicotinamide	ADMA
	S7P	Taurocholate	3-Aminoisobutyrate
	Glycogen	Isethionate	2-Hydroxybutyrate
	Val	UDP-glucuronate	
	Thr	5-Methylthioadenosine	
Lipid	Acylcarnitine (AC)		Fatty acid (FA)
	Triacylglycerol (TG)		Phosphatidylethanolamine (PE)
			Phosphatidylserine (PS)
			Bis(monoacylglycero)phosphate (BMP)
			Lysophosphatidylcholine (LPC)
			Lysophosphatidylinositol (LPI)
			Ceramide (Cer)
			Sphingomyelin (SM)

ATP, G6P, PEP, citrate, 6-phosphogluconate, phosphoenolpyruvate (PEP), sedoheptulose-7-phosphate (S7P) and reduced glutathione. 21 metabolites showed higher abundances in WT mice than in *ob/ob* mice, most of which were non-proteinogenic amino acids. Of 16 lipids, triglyceride (TG) and acylcarnitine (AC) showed higher abundances in *ob/ob* mice than in WT mice, and 8 lipids, including lysophosphatidylcholine (LPC) and fatty acid (FA), showed higher abundances in WT mice than in *ob/ob* mice.

3.3 Identification of glucose-responsive genes and inference of regulatory connections between TFs and genes

The time courses of transcriptomic changes in 14,292 genes in the liver of WT and *ob/ob* mice after oral glucose administration were measured using RNA sequencing (RNA-seq) (Fig. 7, Table 4). I identified glucose-responsive genes in the liver of WT and *ob/ob* mice that show significant changes by oral glucose administration (Fig. 7), and performed pathway enrichment analysis of the glucose-responsive genes (Table 4). To confirm that the glucose-responsive genes show smaller changes or no changes to water administration, I measured the expression of some of the glucose-responsive genes involved in glycolysis, gluconeogenesis, lipid synthesis, and cholesterol synthesis. Most of the glucose-responsive genes showed smaller responses or no responses to oral water administration, except for decreased genes involved in cholesterol metabolism in *ob/ob* mice (Fig. 8, A and B). In the construction of trans-omic network, glucose-responsive genes encoding metabolic enzymes were placed in the Enzyme layer, and those encoding transcription factors in the TF layer (see Fig. 12).

Similar to the metabolites, only a limited number of genes were commonly regulated in WT mice and *ob/ob* mice: 143 genes (1% of the total quantified genes) were upregulated and 163 (1%) were downregulated in both mice (Fig. 7B). Genes upregulated commonly in both mice included fatty acid synthase (*Fasn*) (Fig. 7C). Downregulated genes in both mice included glucose-6-phosphatase (*G6pc*), a key metabolic enzyme of gluconeogenesis (*Gl*).

The number of *ob/ob* mice-specific glucose-responsive genes (1933 = 791 increased + 1142 decreased) is larger than that of WT mice-specific glucose-responsive genes (677 = 327 increased + 350 decreased).

Pathway enrichment analysis showed that the 327 WT mice-specific upregulated genes were enriched in steroid biosynthesis (Table 4). Furthermore, 168 genes that were upregulated in WT mice and downregulated in *ob/ob* mice were enriched in cholesterol synthesis (steroid biosynthesis and terpenoid backbone synthesis), including 3-hydroxy-3-methylglutaryl CoA synthase 1 (*Hmgcs1*) and acyl-CoA: cholesterol acyltransferase 2 (*Acat2*) (Fig. 7C, pink boxes). The responses of the upregulated genes in cholesterol synthesis were rapid and transient. The WT mice-specific upregulated genes also included ATP-citrate lyase (*Achy*), the gene of the metabolic enzyme which produces cytosolic acetyl-CoA and oxaloacetate. Cytosolic acetyl-CoA is the building block for de novo synthesis of fatty acids and sterols.

No pathway was enriched in 791 *ob/ob* mice-specific upregulated genes. However, these genes included in glycolysis, such as glyceraldehyde-3-phosphate dehydrogenase (*Gapdh*) and pyruvate kinase (*Pklr*), and in lipid synthesis, such as glycerol-3-phosphate dehydrogenase 2 (*Gpd2*) and acetyl-CoA carboxylase beta (*Acacb*) (Fig. 7C). *Gpd1* increased in expression in *ob/ob* mice, but decreased in the WT mice (pink box). *Gpd1*, *Acat2*, and *Hmgcs1* are notable, because these genes showed opposed directions of regulation WT mice and *ob/ob* mice. The metabolism of linoleic acid, arachidonic acid, and vitamin A (retinol metabolism) were enriched in the downregulated genes in the WT mice (Table 4). Genes associated with ribosome were the most significantly enriched in the *ob/ob* mice-specific downregulated genes (Table 4), indicating that overall protein synthesis in the liver was decreased in response to glucose administration in the obese state.

To elucidate the regulatory network of the glucose-responsive genes, I inferred the regulatory links between transcription factors and genes using hierarchical clustering analysis of gene expression time courses together with bioinformatic analysis of transcription factor binding motifs in the TRANSFAC database (41, 42) (Fig. 7C and 9). In brief, we defined a transcription factor whose binding motifs are enriched in the promoter regions of the genes in a cluster, as a common transcription factor of the genes in the cluster. For example, sterol regulatory element binding factor (*Srebf*) was identified as a transcription factor regulating some of the WT mice-specific upregulated genes, and early growth response (*EGR1*) was identified as that regulating some of the *ob/ob* mice-specific upregulated genes (Fig. 7C). I compared the inferred regulatory links between transcription factors and genes with those predicted from chromatin immunoprecipitation (ChIP) experimental

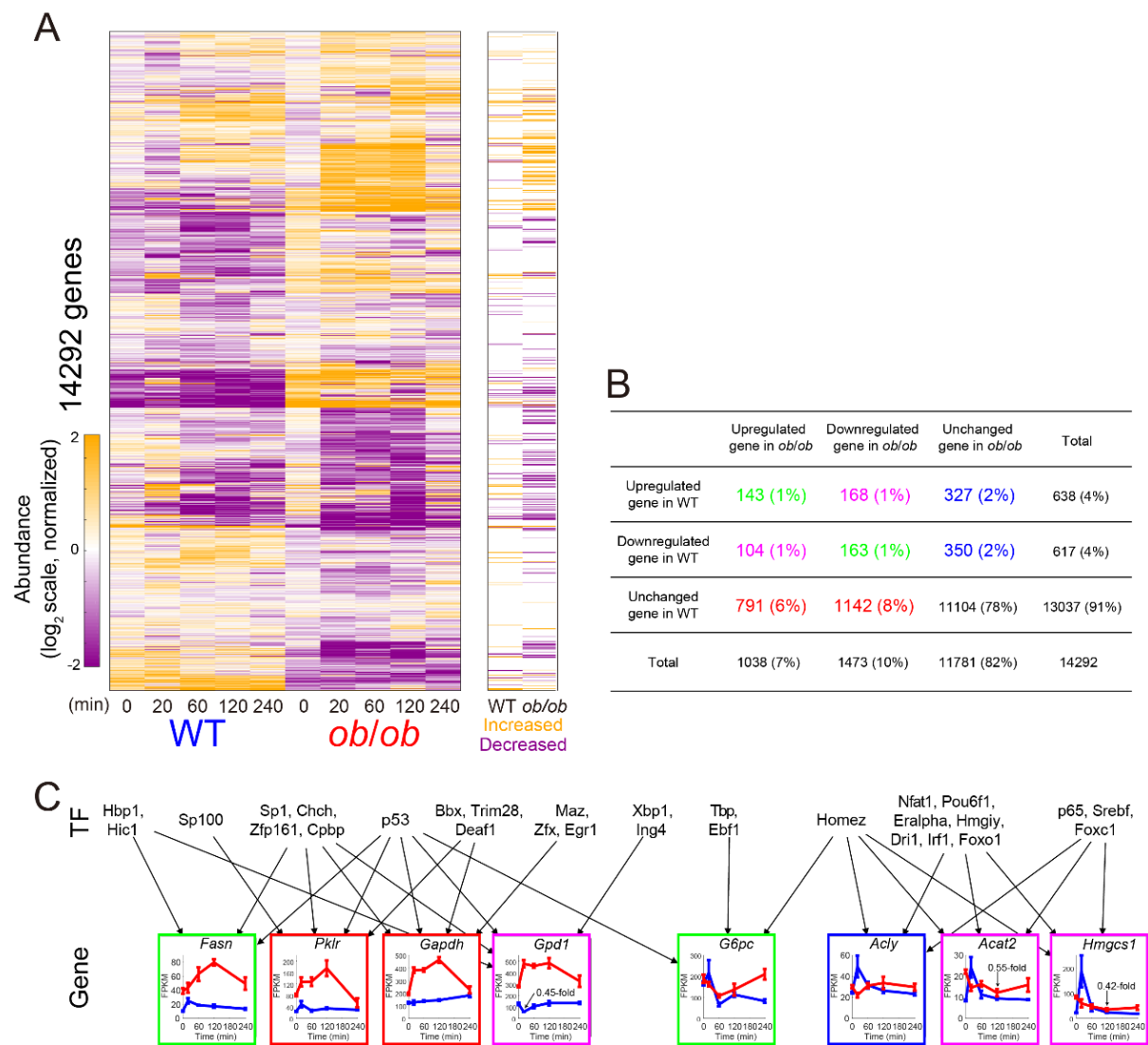


Figure 7. Identification of glucose-responsive genes.

(A) Left: The heat map of the time courses of transcript abundance for 14,292 genes in the livers of WT and *ob/ob* mice following oral glucose administration. To investigate the changes from fasting state, two time courses of each metabolite were divided by the geometric mean of the values of WT mice and *ob/ob* mice in fasting state (0 min), and then log₂-transformed. Genes were ordered by hierarchical clustering using Euclidean distance and Ward's method. Right: The bars in the heat map are colored according to the glucose responsiveness, meaning the change from fasting state (0 min), in the WT and *ob/ob* mice. Genes that showed an absolute log₂ fold change larger than 0.585 ($2^{0.585} = 1.5$) and a q value less than 0.1 at any time point were defined as glucose-responsive: increased (orange), decreased (purple), or were unchanged (white). (B) Upregulated, downregulated, and unchanged genes in the liver of WT mice (row) and *ob/ob* mice: blue, WT specific; red, *ob/ob* specific; green, glucose-responsive metabolites common to both; pink, opposite responses between WT mice and *ob/ob* mice. The number of each type of glucose-responsive genes and their percentages out of the total quantified genes are shown. (C) Graphs showing the gene expression time courses for the indicated genes. Genes include those that exhibited changes in common to both WT and *ob/ob* (green boxes), changes specific to WT mice (blue boxes), changes specific to *ob/ob* mice (red boxes), and changes in opposite directions in each (pink boxes). Within the graphs, blue lines are the responses of the WT mice and red lines are the responses of the *ob/ob* mice. Data are shown as the mean and SEM of mice (n = 11 or 12 at 0 min, n = 3 at 20 min, n = 3 at 60 min, n = 3 at 120 min, and n = 3 at 240 min). The inferred regulatory connections are shown as arrows from transcription factors to genes. The regulatory connections were inferred using hierarchical clustering analysis of gene expression time courses together with a transcription factor database TRANSFAC (41, 42). See Fig. 9 for statistical confidence in inferred transcription factors.

Table 4. Pathway enrichment analysis of the glucose-responsive genes.

Pathways with p value < 0.001 are shown.

	Upregulated gene in <i>ob/ob</i>		Downregulated gene in <i>ob/ob</i>		Unchanged gene in <i>ob/ob</i>	
	activity	p value	activity	p value	activity	p value
Upregulated gene in WT	p53 signaling pathway	3.2×10^{-5}	Terpenoid backbone biosynthesis	2.8×10^{-9}	Metabolic pathways	9.0×10^{-9}
			Steroid biosynthesis	1.8×10^{-8}	Steroid biosynthesis	2.2×10^{-5}
			Metabolic pathways	1.9×10^{-4}	Drug metabolism - cytochrome P450	1.7×10^{-4}
					Glutathione metabolism	5.3×10^{-4}
					Retinol metabolism	9.0×10^{-4}
Downregulated gene in WT	Retinol metabolism	1.3×10^{-4}			Linoleic acid metabolism	2.9×10^{-6}
	Steroid hormone biosynthesis	8.9×10^{-4}			Arachidonic acid metabolism	3.5×10^{-6}
	Linoleic acid metabolism	9.6×10^{-4}			Retinol metabolism	2.5×10^{-4}
Unchanged gene in WT			Ribosome	1.6×10^{-16}		
			Phagosome	2.6×10^{-4}		

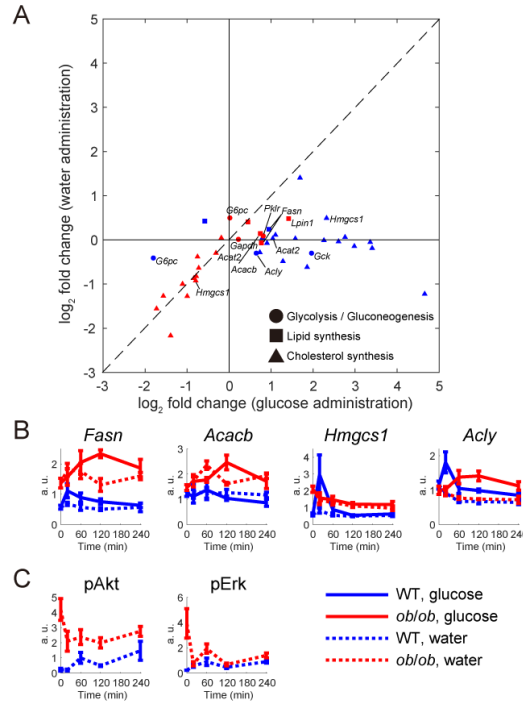


Figure 8. Responses of glucose-responsive molecules during oral water administration.

(A) Responses of glucose-responsive genes to oral glucose administration and oral water administration in WT mice (blue) and *ob/ob* mice (red) measured by RT-PCR. The fold change of the mean amount at a significantly changed time point over the mean amount in fasting state was plotted for each gene. Genes near dashed line indicate that their expression following water administration was similar to the expression of those to glucose administration. The shapes of dots indicate the glucose-responsive genes in glycolysis and gluconeogenesis (circle), lipid synthesis (square), and cholesterol synthesis (triangle) (Table 1). The significantly changed time points were determined from transcriptomic data. If a glucose-responsive gene had multiple significantly changed time points, only the maximum fold change was plotted for the upregulated gene, and only the minimum fold change was plotted for the downregulated gene. (B) Time courses of the indicated changes in gene expression in the liver of WT mice and *ob/ob* mice following oral glucose administration and water glucose administration measured by RT-PCR. The means and SEMs of mice are shown ($n = 5$ for glucose administration, $n = 3$ for water administration). (C) Time courses of the phosphorylation of Akt and Erk in the liver of WT mice and *ob/ob* mice following oral water administration. The means and SEMs of 3 mice are shown.

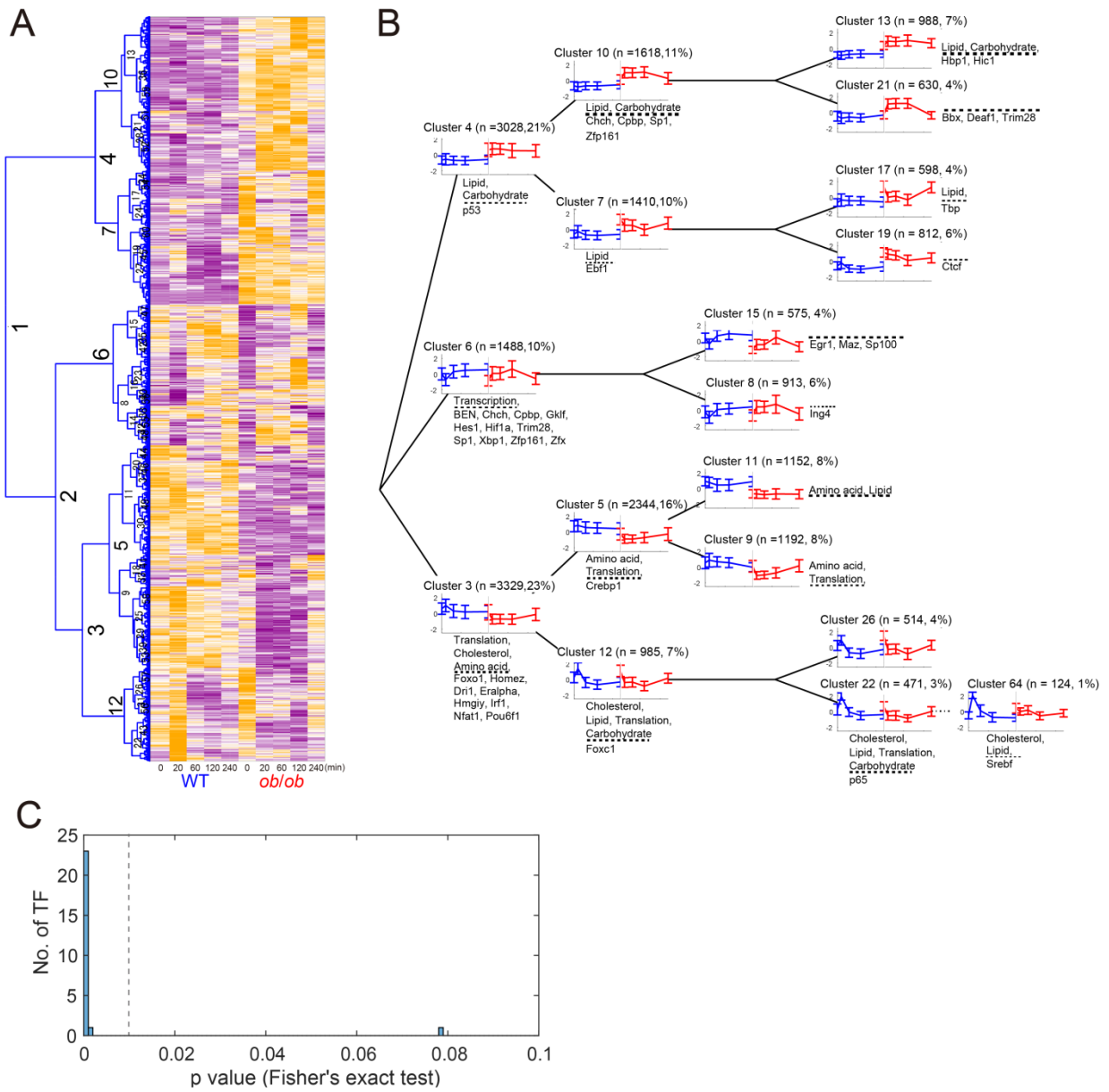


Figure 9. Hierarchical clustering of time courses of gene expression in the liver and inference of regulatory connections between TFs and genes.

(A) The heat map and hierarchical clustering of the Z-score normalized time courses of gene expressions in the liver of WT and *ob/ob* mice following oral glucose administration. The hierarchical clustering was performed using Euclidean distance and Ward's method. The numbers on the tree diagram indicates the cluster identity. Each cluster includes only the genes that show a significant response at any time point either in WT mice or *ob/ob* mice or significant differences between WT mice and *ob/ob* mice at any time point (see Materials and Methods: Clustering analysis). These genes were determined by statistical test. (B) The averaged time courses of the gene expressions for each cluster of WT mice (blue) and *ob/ob* mice (red). The mean and standard deviation of the time courses of gene expressions in the cluster are shown. The time courses are presented on the tree diagram of hierarchical clustering. Significantly enriched pathways (above dashed line, p value < 0.01) and transcription factor motifs (below dashed line, q value < 0.1) in the cluster are described with the time courses. According to the enriched transcription factor motifs, I defined the regulatory connections between the transcription factors and the genes in the cluster. To avoid overestimation, I examined the enrichment of transcription factor binding motif in two children clusters of a cluster, and excluded the parent cluster from the inference if the transcription factor binding motif was significantly enriched in one of the two children clusters. The remaining transcription factor motifs, but not the excluded transcription factor motifs, are described here (above dashed line). The transcription factor motifs enriched in the upstream clusters are not described in the downstream clusters. Metabolic pathways described here are carbohydrate metabolism, amino acid metabolism, lipid metabolism, and cholesterol metabolism (below dashed line). Cholesterol metabolism is indicated by terpenoid backbone biosynthesis and steroid biosynthesis. (C) The histogram of the p values for the overlaps between the inferred genes of the transcription factors and those predicted from ChIP data. The ChIP data were obtained from the ChIP-Atlas database (44). The p values were calculated by one-tailed Fisher's exact test.

Table 5. Pathway enrichment analysis of the genes showing the differences in the amounts of expression between WT mice and *ob/ob* mice before oral glucose administration.

Pathways with p value < 0.001 are shown.

	activity	p value
Larger in <i>ob/ob</i> mice	Glutathione metabolism	2.8×10^{-8}
	Metabolic pathways	4.0×10^{-8}
	Phagosome	8.5×10^{-8}
	Steroid biosynthesis	5.9×10^{-7}
	Metabolism of xenobiotics by cytochrome P450	6.1×10^{-7}
	Drug metabolism - cytochrome P450	2.2×10^{-6}
	Fatty acid elongation	6.7×10^{-5}
	Glycolysis / Gluconeogenesis	5.9×10^{-4}
	Terpenoid backbone biosynthesis	7.5×10^{-4}
Larger in WT mice	Arachidonic acid metabolism	1.4×10^{-5}
	Tryptophan metabolism	6.3×10^{-5}
	Retinol metabolism	6.6×10^{-5}
	Phenylalanine metabolism	1.9×10^{-4}
	Steroid hormone biosynthesis	3.0×10^{-4}

data in the ChIP-Atlas database (44), and confirmed that the inferred links significantly overlapped with those predicted from ChIP data in most TF (Fig. 9C). In the construction of trans-omic networks, the inferred regulatory links between glucose-responsive transcription factors and glucose-responsive genes encoding metabolic enzymes served as the inter-layer regulatory connections between the TF layer and the Enzyme layer (see Fig. 12).

I also identified the significant differences of gene expression between WT mice and *ob/ob* mice before oral glucose administration (Table 5). 1474 genes (10% of the total quantified genes) showed higher expressions in *ob/ob* mice than in WT mice, and these were enriched in glutathione metabolism, glycolysis, and cholesterol synthesis. 708 (5%) showed higher expressions in WT mice than in *ob/ob* mice, and the enriched pathway included two amino acid metabolic pathways (tryptophan metabolism and phenylalanine metabolism).

3.4 Identification of glucose-responsive phosphorylation of insulin signaling molecules

Many metabolic reactions are regulated either by enzyme phosphorylation or by transcription factor phosphorylation regulating gene expression of enzymes. Phosphorylation of enzymes and transcription factors are regulated by signaling molecules. Glucose stimulates the release of insulin in pancreas, followed by the activation of insulin signaling pathway in the liver, including phosphorylation of some enzymes and transcription factors. Thus, I measured the amount and phosphorylation of enzymes, transcription factors, and signaling molecules in the insulin signaling pathway by Western blotting, and identified glucose-responsive phosphorylation of insulin signaling molecules in the liver of WT and *ob/ob* mice (Figs. 10 and 11).

Common responses were phosphorylation of Erk and ribosomal protein S6 and dephosphorylation of glycogen phosphorylase (Gp) and glycogen synthase (Gs), indicating the activation of protein synthesis and glycogen production. Phosphorylation of insulin receptor β (Ir β), Akt, forkhead box protein O1 (Foxo1), and glycogen synthase kinase 3 β (Gsk3 β) transiently increased in WT mice but not in *ob/ob* mice. Changes in opposite directions between WT and *ob/ob* mice were observed in the amount of insulin receptor substrate 1 and 2 (Irs1 and Irs2), and phosphorylation of Ir β and Irs1. These opposite changes at the early parts of the insulin pathway could contribute to the diverse responses at the late parts of pathway, such as WT mice-

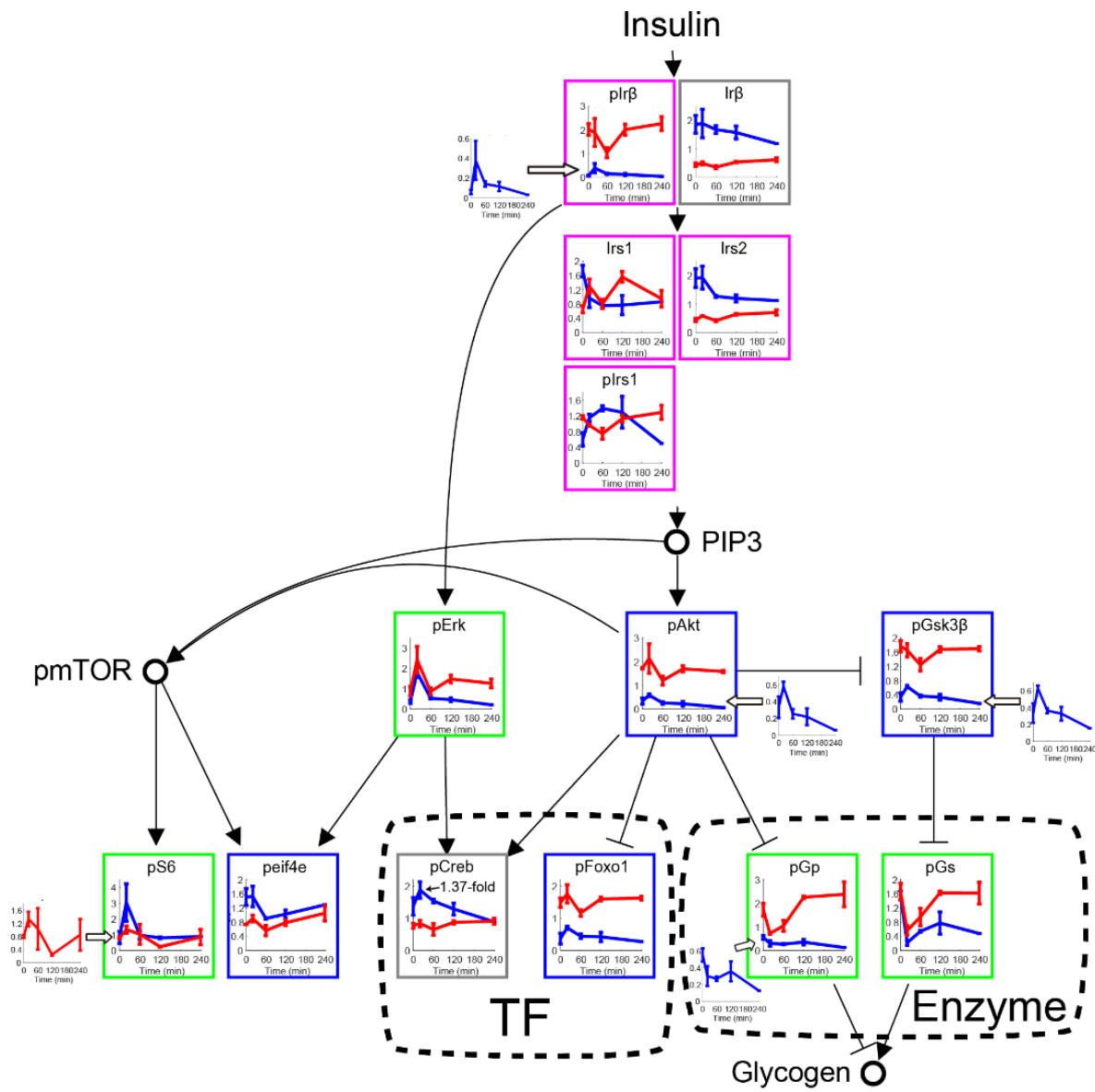


Figure 10. Identification of glucose-responsive phosphorylation of insulin signaling molecules.

Time courses of the amount and phosphorylation of the indicated insulin signaling molecules in the liver of WT mice (blue lines) and *ob/ob* mice (red lines) following oral glucose administration. Phosphorylated proteins are indicated by the prefix “p” (for example, phosphorylated Erk, pErk). Data are shown as the mean and SEM of 3 mice except for WT samples for 3 time points, which had inconsistent loading (see Fig. 11 for Western blot). The time course graphs are presented in the context of the insulin signaling pathway from the KEGG database (37, 38). Edges may reflect direct or indirect regulatory events. Not all molecules in this pathway are shown. The nodes that are presented as circles [phosphatidyl-inositol 3,4,5-trisphosphate (PIP3) and mammalian target of rapamycin (mTor)] were not quantified here. The colors of the boxes around each graph indicate a change in amount or phosphorylation specific to WT (blue), specific to *ob/ob* (red), common to both (green), opposite between WT mice and *ob/ob* (pink). Proteins that did not exhibit a change in amount or phosphorylation are outlined in gray. Proteins that showed an absolute \log_2 fold change larger than 0.585 ($2^{0.585} = 1.5$) at any time point were defined as glucose-responsive. Glucose-responsive molecules in the TF and Enzyme layers are enclosed in dashed boxes.

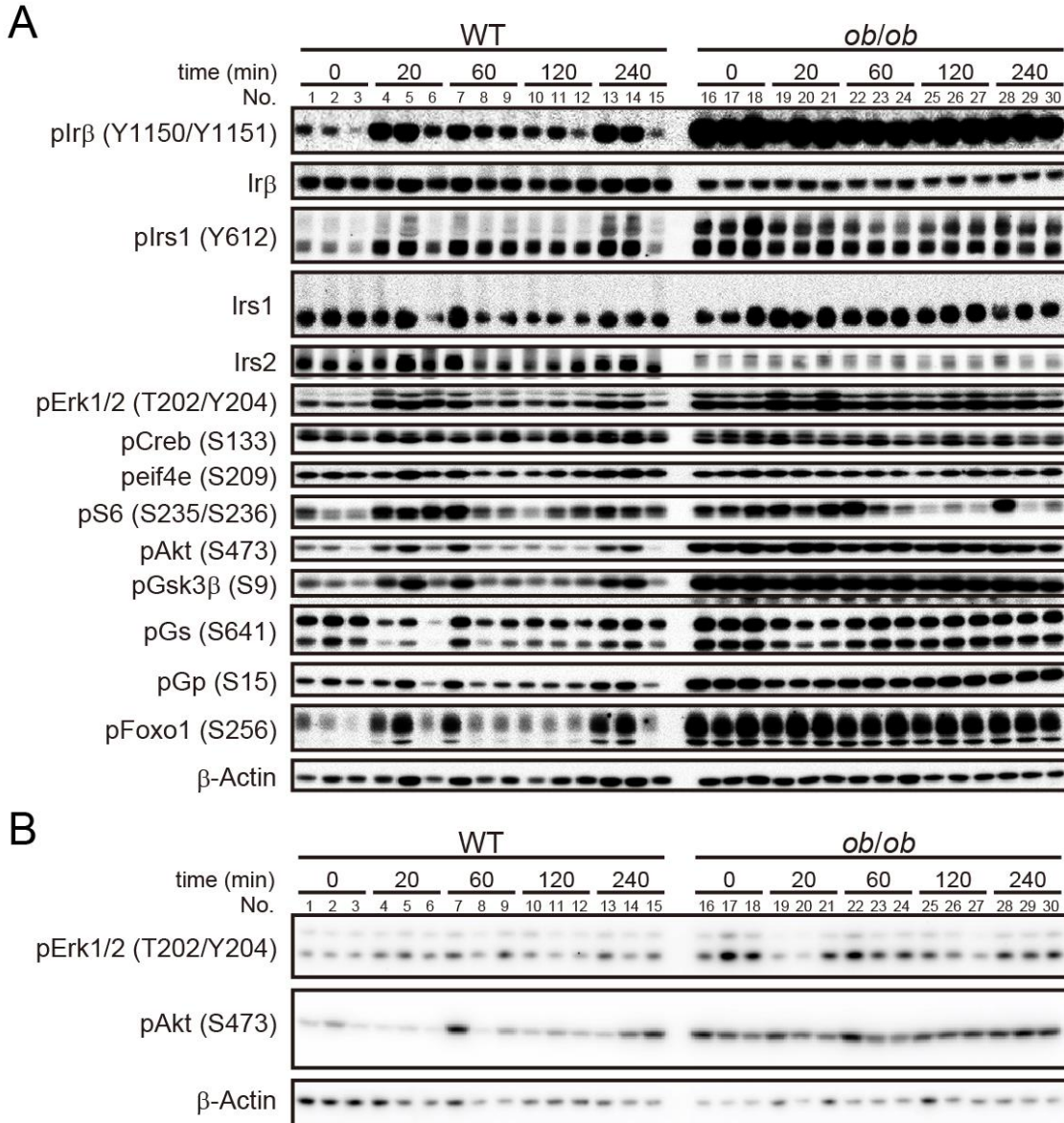


Figure 11. Western blotting for insulin signaling molecules.

The amount and phosphorylation of the indicated insulin signaling molecules in the liver of WT mice and *ob/ob* mice at the indicated time point after oral glucose administration (**A**) and oral water administration (**B**).

- 5 Residues in parentheses indicate the phosphorylation site(s) (human sequence numbering) recognized by the antibodies. All Western blot data for 3 mice are shown. In panel A, Lanes 5, 7, 13 and 14 were excluded in the following analysis, because the β -actin loading control for each indicated inconsistency from the other WT samples.

specific phosphorylation of Akt. I confirmed that the phosphorylation of Akt and Erk did not increase after oral water administration (Fig. 8C). In the construction of trans-omic networks, pGs and pGp were placed in the Enzyme layer, pFoxo1 in the TF layer, and the others in the Insulin signal layer (see Fig. 12).

I also identified the significant differences of the amounts and phosphorylation of signaling molecules between WT mice and *ob/ob* mice before oral glucose administration. The phosphorylation of Irβ, Akt, Foxo1, Gsk3β, and Gp were significantly higher in *ob/ob* mice than WT mice, consistent with the higher concentration of blood insulin in *ob/ob* mice (Fig. 3A). The amount of Irβ was lower in *ob/ob* mice than in WT mice.

3.5 The construction of regulatory trans-omic network for glucose-responsive metabolic reactions

Using the glucose-responsive molecules and the inferred regulatory connection between TF and genes, I constructed the regulatory trans-omic networks for glucose-responsive metabolic reactions of WT mice and *ob/ob* mice, which consists of five layers— Insulin signal, TF, Enzyme, Reaction, and Metabolite— and regulatory connections between the layers (Fig. 12, A and B). The Insulin signal layer contains signaling molecules showing glucose-responsive phosphorylation. The TF layer contains the “glucose-responsive transcription factors”, defined as the transcription factors encoded by glucose-responsive genes or those showing glucose-responsive phosphorylation. The Enzyme layer contains the “glucose-responsive metabolic enzymes”, defined as the metabolic enzymes encoded by glucose-responsive genes or those showing glucose-responsive phosphorylation. The Reaction layer contains the “glucose-responsive metabolic reactions”, defined as metabolic reactions regulated by the glucose-responsive metabolites and/or glucose-responsive metabolic enzymes. For instance, dephosphorylation of G6P (EC 3.1.3.9) was identified as a common glucose-responsive metabolic reaction in both mice, because dephosphorylation of G6P was regulated by G6P, a common glucose-responsive metabolite, and by *G6pc*, a common glucose-responsive gene (Fig. 1). The Metabolite layer contains glucose-responsive metabolites. Using the information from the liver analysis, I colored the nodes in each layer according to the type of responses; common changes in both WT and *ob/ob* mice, WT mice-specific changes, *ob/ob* mice-specific changes, opposing changed between WT mice and *ob/ob* mice.

Then, inter-layer regulatory connections between glucose-responsive molecules were determined based on several databases and the inferred network. The inter-layer connections from the Insulin signal layer to the TF layer and to the Enzyme layer were determined according to the regulation of transcription factors or enzymes by kinases in the KEGG database (37, 38). The inter-layer connections from the TF layer to the Enzyme layer were based on the inferred regulatory connections between genes and transcription factors. Note that, among all the inferred regulatory connections, only those between glucose-responsive transcription factors and glucose-responsive genes encoding enzymes are included. The inter-layer connections from the Enzyme layer to the Reaction layer were determined by matching enzymes to their corresponding reactions according to the KEGG database (37, 38). The inter-layer connections from the Metabolite layer to the reaction layer consisted of two types of regulation: regulatory connections mediated by allosteric regulators and those mediated by the substrate or product of the reaction. Allosteric regulatory connections were determined according to the BRENDA database (45), and substrate or product-mediated regulatory connections were determined according to the KEGG database (37, 38). This trans-omic network contains the regulatory connections for each metabolic pathway, such as glycolysis (Fig. 18), glycogen metabolism (Fig. 19), lipid synthesis (Fig. 20), and cholesterol synthesis (Fig. 25).

Comparison of the regulatory trans-omic networks for glucose-responsive metabolic reactions between WT and *ob/ob* mice allowed us to identify WT mice-specific (Fig. 12B, blue), *ob/ob* mice-specific (Fig. 12B, red), and common (Fig. 12B, green) glucose-responsive molecules and inter-layer regulatory connections. As a whole, the numbers of WT mice-specific glucose-responsive molecules were larger than that of *ob/ob* mice-specific molecules except for glucose-responsive gene in Enzyme layer (Fig. 12B). The number of WT mice-specific inter-layer regulatory connections between the Metabolite layer and the Reaction layer was also much greater than those in the *ob/ob* mice-specific connections, suggesting that the response to glucose is dominated by metabolites in the healthy state. In contrast, the *ob/ob*-specific glucose-responsive molecules in the Enzyme layer and the number of *ob/ob*-specific inter-layer connections between the Enzyme layer and the Reaction layer were greater than those of WT mice, indicating the large alteration in the transcriptional regulation of metabolism in the obese state.

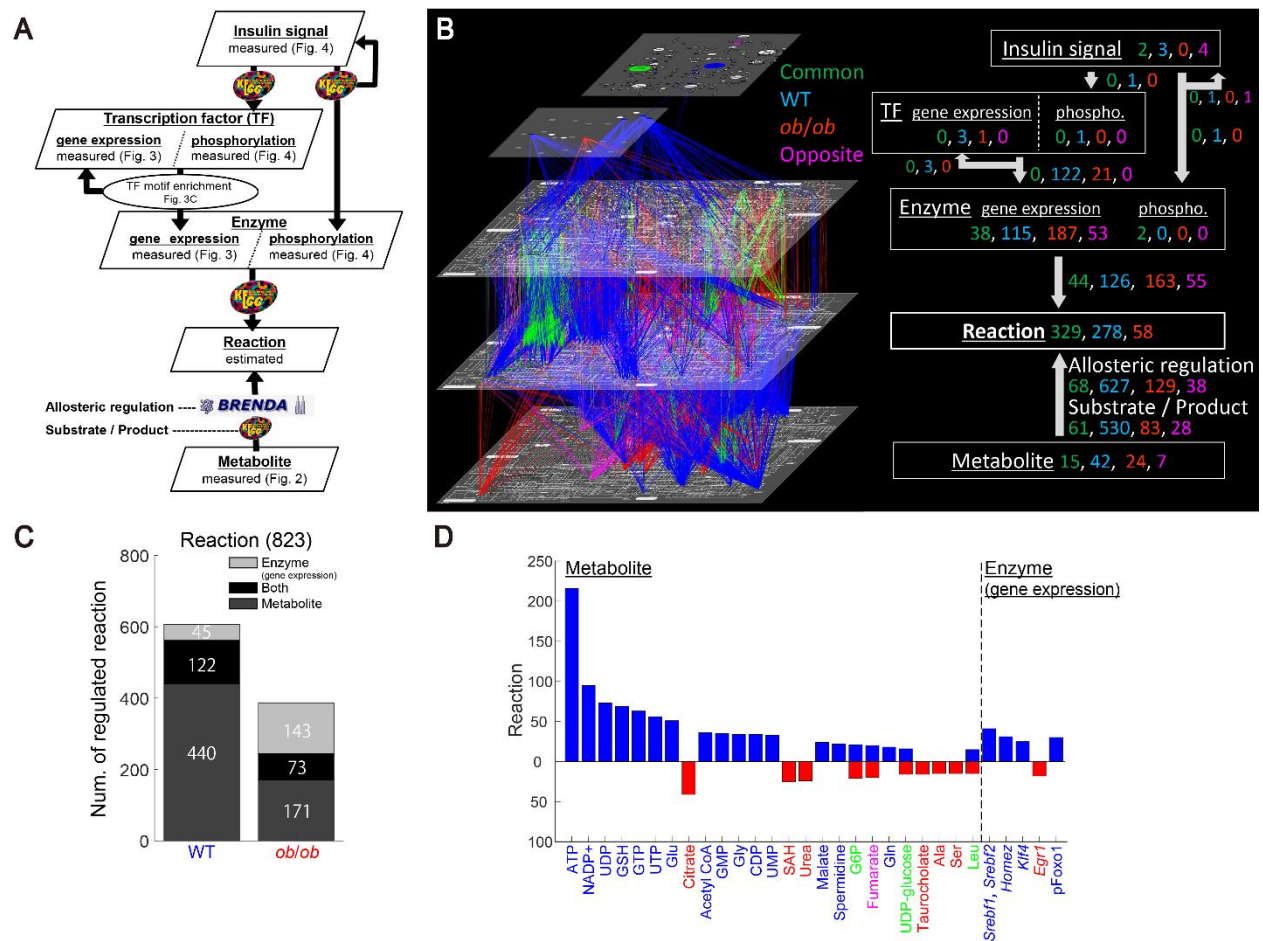


Figure 12. The construction of regulatory trans-omic network for glucose-responsive metabolic reactions.

(A) The procedure for constructing the regulatory trans-omic network for glucose-responsive metabolic reactions. The layers of Insulin signal, Transcription factor (TF), Enzyme, and Metabolite correspond to glucose-responsive molecules. The Reaction layer represents “glucose-responsive metabolic reactions”, which are defined as metabolic reaction regulated by the glucose-responsive molecules. The upward and downward arrows indicate inter-layer regulatory connections, and the recurrent arrows indicate intra-layer regulatory events. The databases used to identify the inter- and intra-layer regulatory connections are shown on the arrows. (B) The regulatory trans-omic network for glucose-responsive metabolic reactions. The left diagram represents the network as colored nodes in the layers and edges between the layers with colored nodes representing glucose-responsive molecules and colored edges representing inter-layer regulatory connections: green, glucose-responsive molecules and inter-layer regulation common in both WT and *ob/ob* mice; blue, specific to WT mice; red, specific to *ob/ob* mice; pink, opposite responses between WT mice and *ob/ob* mice. A common or an opposite regulatory connection was defined if the regulating molecule of the connection is common or opposite, respectively. The numbers of each type of glucose-responsive node and edge are shown with the same colors in the network summary to the right. The Insulin signal layer is the insulin signaling pathway constructed in a previous phosphoproteomic study (18). The Enzyme, Reaction, and Metabolite layers are organized into global metabolic pathway (mmu01100) in the KEGG database (37, 38). Phospho, phosphorylation. (C) The number of glucose-responsive metabolic reactions regulated by glucose-responsive molecules in the enzyme layer or the metabolite layer or both from a total of 823 metabolic reactions in the liver. (D) The number of glucose-responsive metabolic reactions regulated by the indicated glucose-responsive molecules in WT mice (upper, blue) and *ob/ob* mice (lower, red). The colors of the names of molecules indicate the type of glucose-responsive molecules as described in B. Glucose-responsive metabolites that regulated more than 15 metabolic reactions and exhibited significant association with any metabolic pathway (Fig. 15B) are shown. The names of the transcription factors coded by glucose-responsive genes are described in italic type, and those showing glucose-responsive phosphorylation have the prefix “p.”

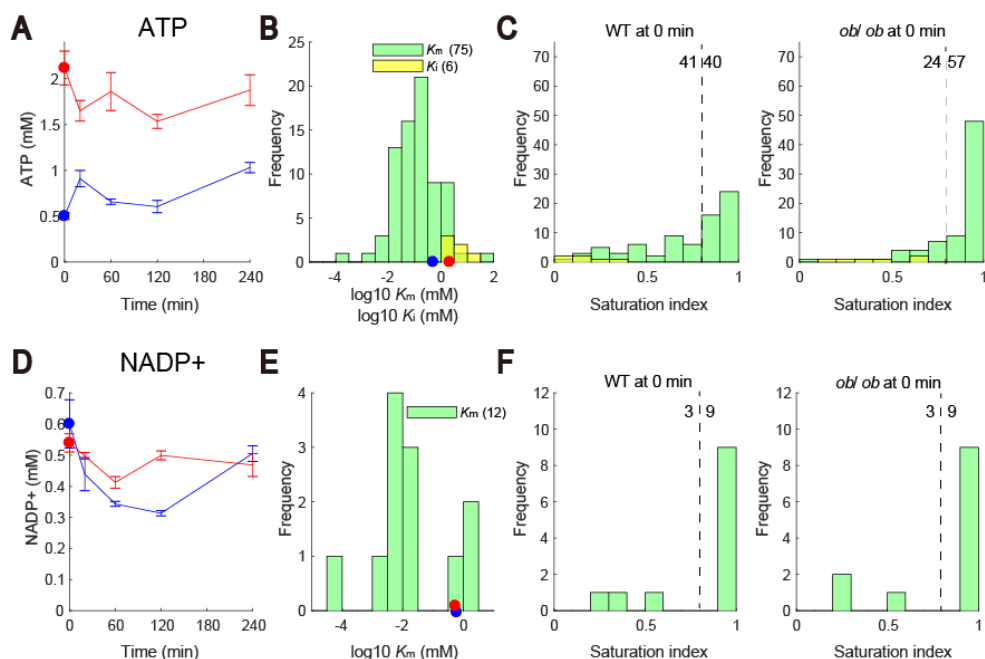


Figure 13. K_m and K_i of metabolic reactions regulated by ATP and NADP+.

(A) Graph of the time courses for ATP in the liver of WT mice (blue) and *ob/ob* mice (red) following oral glucose administration. The means and SEMs of 5 mice are shown. The dots indicate the fasting values. (B)

5 Histogram of K_m values and K_i values of metabolic reactions regulated by ATP according to the BRENDA database (45). The dots indicate the fasting values of ATP in WT mice (blue) and *ob/ob* mice (red). (C)

Histograms of the saturation indices of metabolic reactions regulated by ATP in WT mice and *ob/ob* mice in fasting state (0 min). The saturation indices of metabolic reactions regulated by ATP as substrate/product (green) were defined as $[ATP] / [ATP] + K_m$, and those as allosteric regulator (yellow) were defined as $[ATP] /$

10 $[ATP] + K_i$. Saturation index closer to 1 means higher saturation, and that closer to 0 means lower saturation. I defined unsaturated metabolic reactions as metabolic reactions with saturation indices that were less than 0.8 (dashed line). The numbers besides the dashed lines indicate the numbers of unsaturated metabolic reactions

(left) and saturated metabolic reactions (right). (D) Graph of the time courses for NADP+ in the liver of WT mice (blue) and *ob/ob* mice (red) following oral glucose administration. (E) Histogram of K_m values of

15 metabolic reactions regulated by NADP+ according to the BRENDA database (45). K_i values were not

available in the BRENDA database. (F) Histograms of the saturation indices of metabolic reactions regulated by NADP+ in WT mice and *ob/ob* mice in fasting state (0 min).

I calculated the number of glucose-responsive metabolic reactions that were regulated by glucose-responsive metabolites in the metabolite layer and/or by glucose-responsive genes in the Enzyme layer in WT and *ob/ob* mice after oral glucose administration (Fig. 12, C and D). This analysis showed that metabolite-mediated regulation of metabolism dominates the response to glucose administration in WT mice and that transcriptional regulation play a larger role in metabolic regulation of *ob/ob* mice (Fig. 12C). WT-mice specific glucose-responsive metabolites included cofactors, such as ATP and NADP⁺, and these metabolites regulated a large number of glucose-responsive metabolic reactions (216 reactions by ATP, and 95 reactions by NADP⁺) (Fig. 12D). Because metabolites can effectively change metabolic reactions only when the metabolite concentration is not saturating, I quantitatively evaluated the saturation by comparing metabolite concentration with binding affinity, K_m and K_i , for each metabolic reaction (Fig. 13) to calculate binding site saturation (62). I evaluated the saturation of ATP (Fig. 13A) and NADP⁺ (Fig. 13D) for each metabolic reaction whose binding affinity were available in the BRENDA database (45) (Fig. 13, B and E). We found that, in WT mice, ATP was not saturating in 41 of 81 glucose responsive metabolic reactions regulated by ATP, such as the conversion of F6P to fructose 1,6-bisphosphate (F1,6P) in glycolysis (Fig. 13C), and NADP⁺ was not saturating in 3 of 12 glucose-responsive metabolic reactions regulated by NADP⁺ (Fig. 13F), indicating that many of these inter-layer regulations can be effective in WT mice.

3.6 Differences in the regulatory trans-omic networks between WT and *ob/ob* mice

To extract the critical differences in the regulatory networks of glucose-responsive metabolic reactions between WT and *ob/ob* mice, I condensed the metabolic reactions in the regulatory networks based on the metabolic pathway information through the following steps (Fig. 14). First, I united the metabolic reactions of a metabolic pathway into one “metabolic pathway node” according to the KEGG database, and created a “Pathway” layer with the metabolic pathway nodes and their regulatory connections, instead of the Reaction layer (Fig. 14A). In this step, I excluded metabolic pathway nodes that did not exhibit statistically significant associations with any glucose-responsive molecule (Fig. 15). Then, I classified the glucose-responsive Pathway into 3 classes: carbohydrate, lipid, and amino acid. As a further simplification, I removed less

important glucose-responsive molecules (e.g. enzymes only related to removed metabolic pathway) and inter-layer connections (e.g. connection between pathway and metabolites that regulated fewer than 5 metabolic reactions) (see Method for details). Through this process, I constructed the condensed regulatory trans-omic networks for glucose-responsive metabolic reactions.

5 The condensed regulatory trans-omic network of WT mice has three specific characteristics of the inter-layer regulatory connections (Fig. 14B): (i) from the Insulin signal layer to the TF layer and the Enzyme layer, pAkt was a major signaling molecule that regulated pFoxo1 and pFoxO1-mediated glucose-responsive genes; (ii) from the TF layer to the Enzyme layer, pFoxo1 and the glucose-responsive transcription factor encoded by *Srebf*, *Klf4*, and *Homez* regulated glucose-responsive genes; and (iii) from the Metabolite layer to the Pathway
10 layer, the glucose-responsive metabolites regulate many metabolic pathway nodes, especially in carbohydrate metabolism and amino acid metabolism.

To evaluate the regulatory mechanism for each metabolic pathway, I examined upstream regulators of metabolic pathways by counting the number of glucose-responsive reactions in the pathway (Fig. 15, A and B). Lipid metabolic pathways were regulated by more enzymes encoded by glucose-responsive genes than were
15 carbohydrate metabolic pathways, which was regulated by more metabolites (Fig. 15A). Furthermore, I identified some statistically significant associations between a metabolic pathway and a glucose-responsive molecule (Fig. 15B). For example, *Srebf* was identified as transcription factor that specifically regulated terpenoid backbone biosynthesis and steroid biosynthesis, both of which are metabolic pathways related to cholesterol synthesis. Meanwhile, FoxO1, whose phosphorylation caused the downregulation of its target
20 genes, was identified as the regulator of various types of metabolic pathway.

The inter-layer regulatory connections of *ob/ob* mice also has three specific characteristics (Fig. 14C): (i) from the Insulin signal layer to the TF layer and the Enzyme layer, pErk was a signaling molecule that regulated *Egr1* and *Egr1*-mediated glucose-responsive genes; (ii) from the Enzyme layer to the Pathway layer, most of the regulatory connections are specific to *ob/ob* mice or opposing between WT mice and *ob/ob* mice; and (iii)
25 from the Metabolite layer to the Pathway layer, most of regulations of metabolic pathway nodes by metabolites found in WT mice was absent. The conserved regulatory events between the healthy and obese

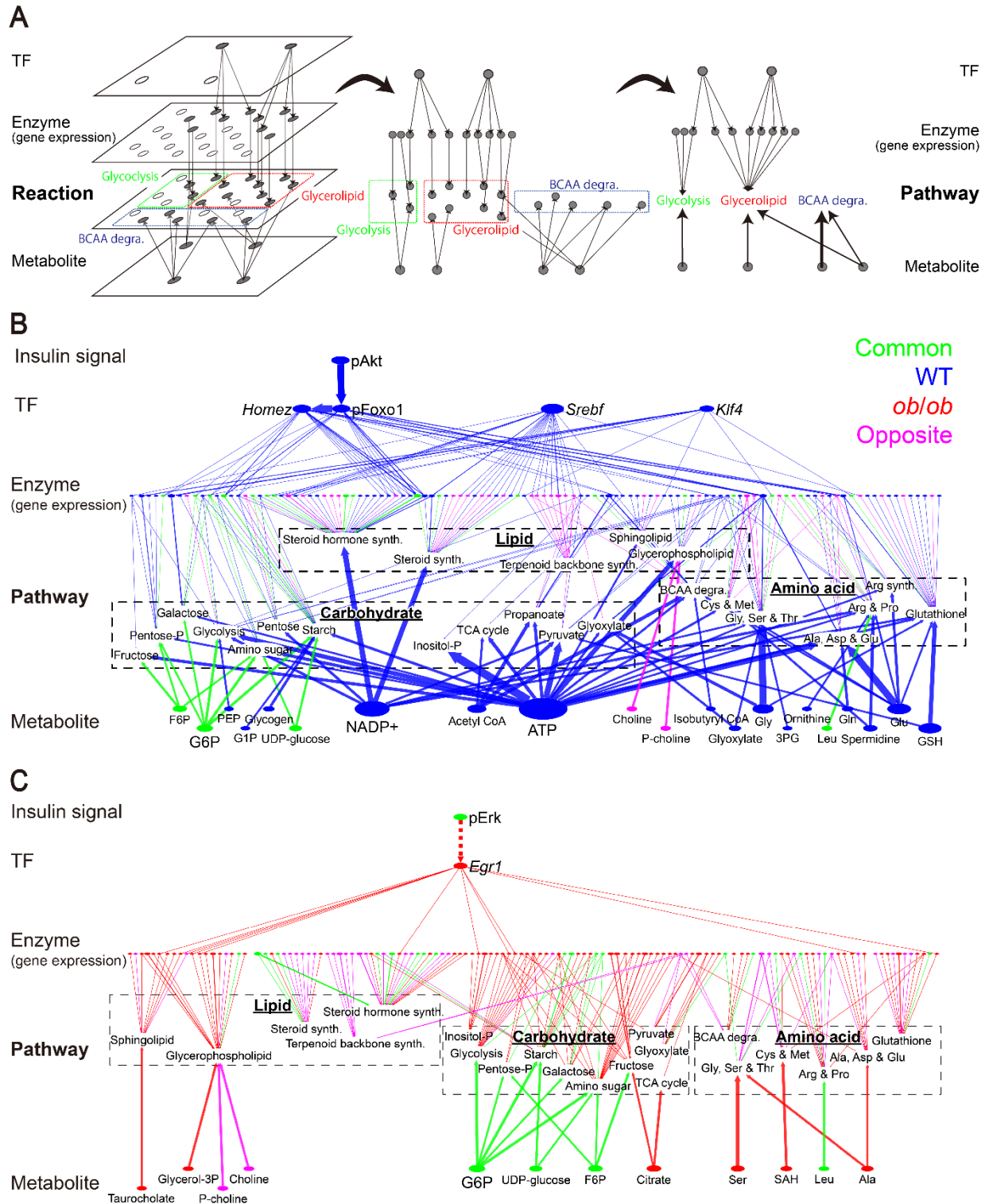


Figure 14. The condensed regulatory trans-omic networks for the liver metabolic response to glucose in the healthy and obese states.

(A) The process of reducing the complexity of the trans-omic network into condensed versions. I grouped related metabolic reactions within a specific metabolic pathway into one “metabolic pathway node,” such as Glycolysis, Glycerolipid, or BCAA degradation, using the metabolic maps in KEGG (37, 38). I then generated a Pathway layer of the metabolic pathway nodes and grouped these nodes into classes of carbohydrate, lipid, or amino acid, according to the KEGG database (37, 38). (B, C) The condensed regulatory trans-omic network of the liver response to glucose in WT and *ob/ob* mice. The color of nodes (glucose-responsive molecules) and edges (inter-layer regulatory connections) indicates the type of molecules and regulations as described in Fig. 12B. Dashed edge between pErk and *Egr1* indicates the indirect regulatory connection (49, 50). In the transcription factor (TF) layer, the names of the transcription factors encoded by glucose-responsive genes are written in italics, and those showing glucose-responsive phosphorylation have the prefix “p.” *Srebf* corresponds to *Srebf1* and *Srebf2*, both of which were glucose-responsive genes specific to WT mice. The Enzyme layer contains only those metabolic enzymes that are regulated by glucose-responsive changes in gene expression, not those regulated only by phosphorylation. Metabolic pathway nodes that exhibited significant associations with any glucose-responsive molecule are included (Fig. 15B). Dashed boxes enclose the nodes for the lipid, carbohydrate, and amino acid classes. Glucose-responsive metabolites that exhibited significant associations with any metabolic pathway are included. The inter-layer regulatory connections from the Metabolite layer to the Pathway layer include only those that regulate 5 or more metabolic reactions. The size of the nodes and the width of the edges indicate the relative number of the regulated metabolic reactions.

(A) For each metabolic pathway node, the percent of regulated metabolic reactions by glucose-responsive metabolites (x-axis) and by glucose-responsive genes of metabolic enzyme (y-axis) is plotted for WT mice and *ob/ob* mice. The size of the dots indicates the number of regulated metabolic reactions in each metabolic pathway node either by glucose-responsive metabolites or genes or both. The colors of the dots indicate the classes of metabolic pathway node according to the KEGG database (37, 38): carbohydrate (green), amino acid (blue), and lipid (red). (B) Heat maps showing the number of regulated metabolic reactions in each metabolic pathway node (rows) by each glucose-responsive metabolite (left columns) and each transcription factor-dependent glucose-responsive genes of metabolic enzymes (right columns) in WT mice and *ob/ob* mice. The signs * indicate the significant associations (p value < 0.05) between metabolic reactions in the metabolic pathway node and those regulated by the glucose-responsive molecules. The p values were calculated by one-tailed Fisher's exact test. Only metabolic pathway nodes with significant associations with any glucose-responsive molecule are shown. Only glucose-responsive metabolites with significant associations with any metabolic pathway node are shown.

states were identified in carbohydrate metabolic reactions, such as the regulation of glycolysis and starch metabolism by G6P (Figs. 18 and 19).

3.7 Differences in temporal control of the regulatory trans-omic network

To examine temporal control of glucose-responsive molecules and inter-layer regulatory connections, I calculated their time constants ($T_{1/2}$), an index of the temporal rate of response (Fig. 16 and Fig. 17). $T_{1/2}$ of a glucose-responsive molecule was defined as the time when the response reached 50% of the maximum amplitude for an increased molecule, or of the minimum amplitude for a decreased molecule (Fig. 16A). $T_{1/2}$ of an inter-layer regulatory connection was defined as the same $T_{1/2}$ of a glucose-responsive molecule that is the regulating molecule of the inter-layer regulatory connection, not the $T_{1/2}$ of the regulated molecule. I defined the responses with $T_{1/2}$ values shorter than 20 min as “rapid”, and those with values longer than 60 min as “slow.” From the Enzyme layer to the Reaction layer, approximately 50% of the inter-layer regulatory connections were rapid in both mice, and the number of the slow inter-layer regulatory connections was approximately 3-times larger in *ob/ob* mice than in WT mice (Fig. 16B and Fig. 17A). From the Metabolite layer to the Reaction layer, most of the inter-layer regulatory connections were rapid in WT mice, and these were largely reduced in *ob/ob* mice.

I also examined the $T_{1/2}$ values of molecules and regulatory connections in the condensed regulatory trans-omic networks (Fig. 16, C and D). In WT mice, most inter-layer regulatory connections were rapid (Fig. 16C). Approximately 50% of the regulatory connections between metabolic reactions and pFoxo1-mediated responsive genes were rapid, and all of the *Srebf*-mediated regulatory connections were rapid (Fig. 17B). In contrast, in *ob/ob* mice, 50% of the inter-layer regulatory connections were slow between *Egr1*-dependent genes from the Enzyme layer to the metabolic reactions in the Pathway layer (Fig. 17B). These results indicated that regulation of glucose-responsive metabolic reactions is different in temporal control, as well as in network structure, between WT mice and *ob/ob* mice, partially caused by the difference of transcription factors.

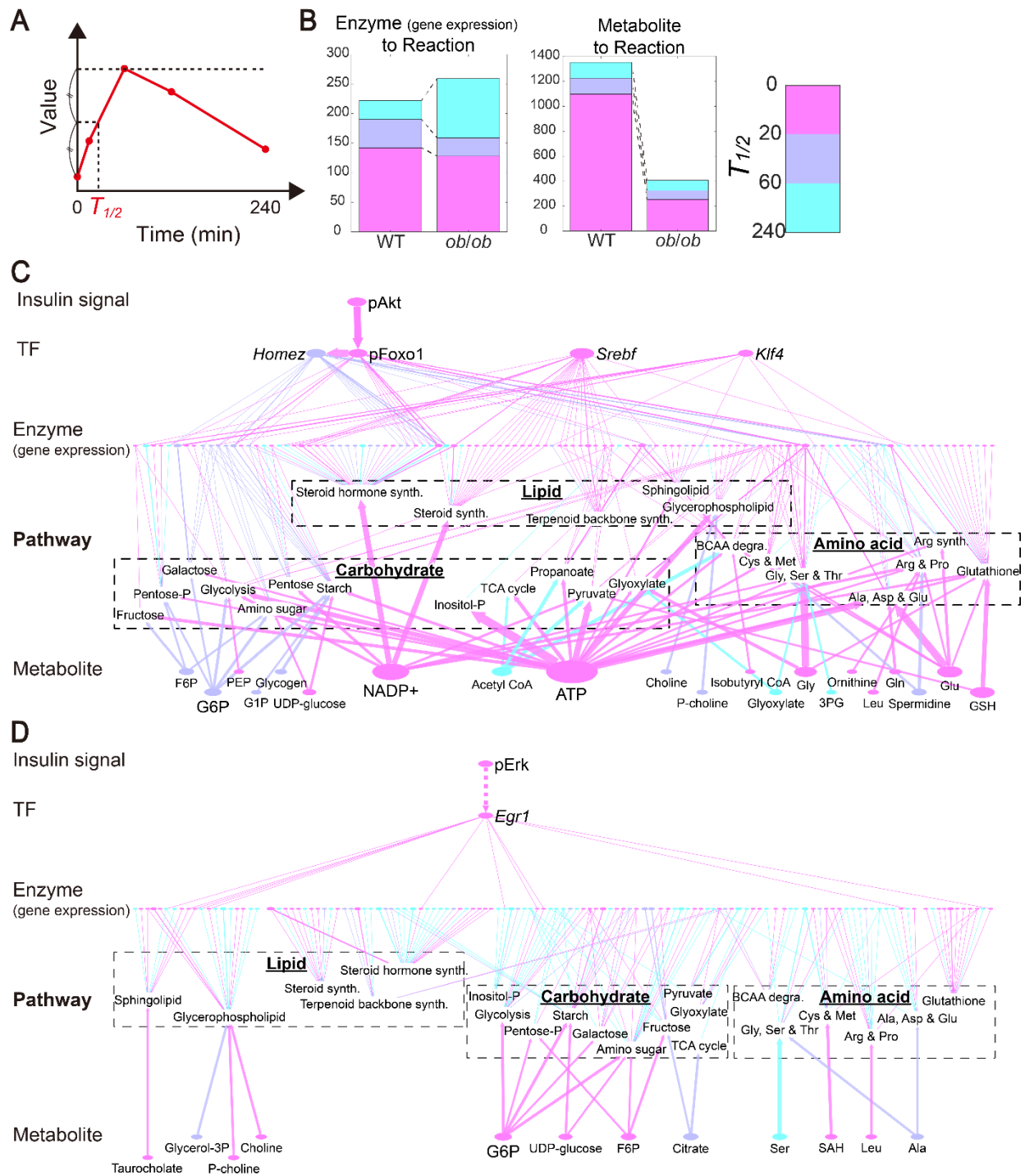


Figure 16. Temporal control of the regulatory trans-omic networks for the liver metabolic response to glucose in the healthy and obese states.

(A) Definition of $T_{1/2}$, an index of the temporal rate of response. (B) The number of the inter-layer regulatory connections with $T_{1/2}$ values in the ranges indicated to the Reaction layer from the Enzyme layer and from the Metabolite layer. (C, D) Temporal control of the condensed regulatory trans-omic network of WT and *ob/ob* mice. The color of nodes (glucose-responsive molecules) and edges (inter-layer regulatory connections)

5 indicates the $T_{1/2}$ value according to the ranges in the color bar in B. *Srebf* corresponds to *Srebf1* and *Srebf2*, both of whose $T_{1/2}$ values were 10 min.

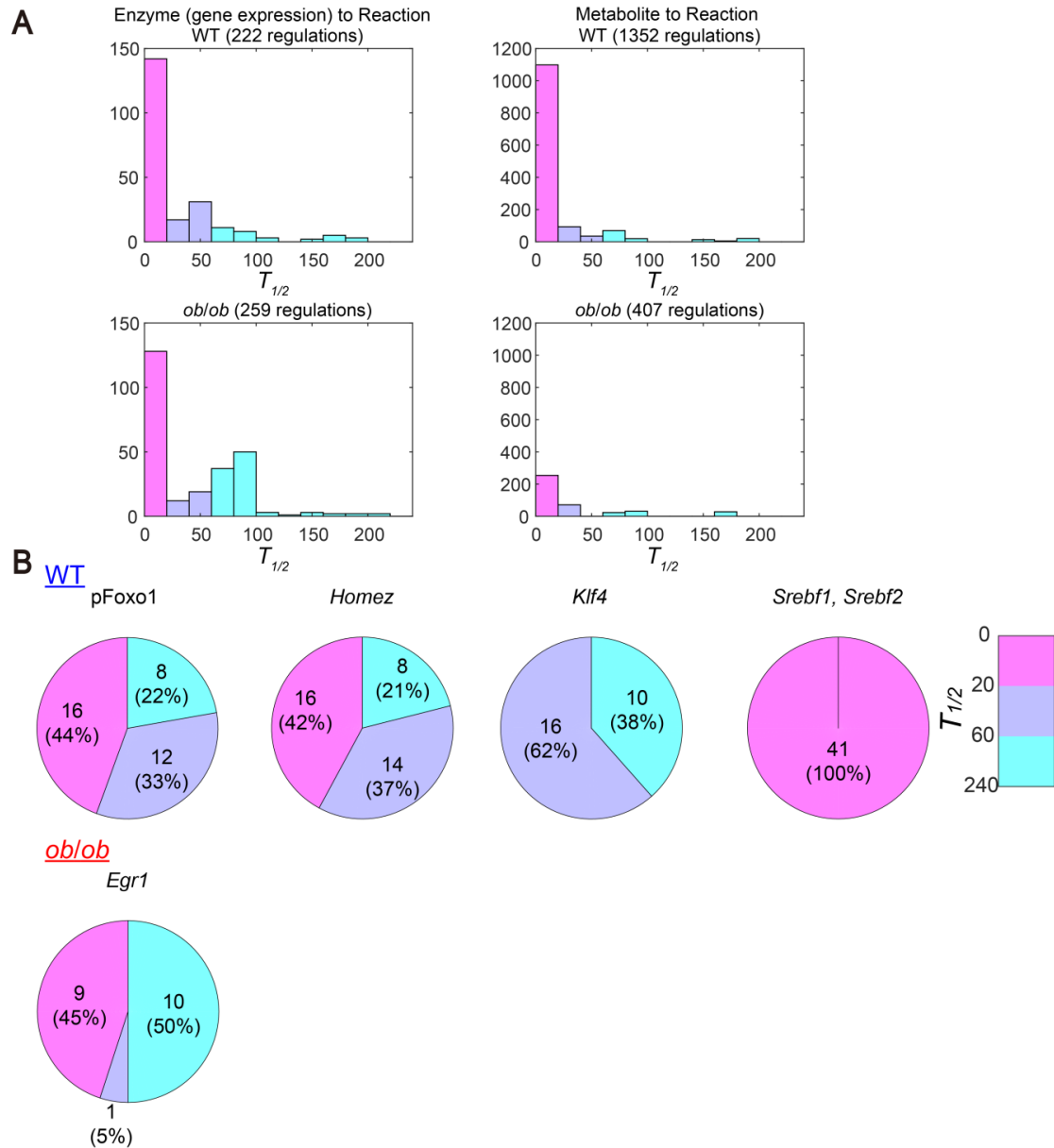


Figure 17. $T_{1/2}$ values of the inter-layer regulatory connections from glucose-responsive molecules to metabolic reactions.

(A) The number of the inter-layer regulatory connections with indicated $T_{1/2}$ values from the Enzyme layer to the Reaction layer and from the Metabolite layer to the Reaction layer in WT mice and *ob/ob* mice. (B) The number and percentage of $T_{1/2}$ values of the inter-layer regulatory connections of metabolic reactions by the indicated transcription factor-dependent glucose-responsive genes encoding metabolic enzymes in WT mice and *ob/ob* mice. The colors of the pies represent the ranges of $T_{1/2}$ values as shown in the color bar on the right.

3.8 The regulatory trans-omic network for glucose-responsive metabolic reactions in carbohydrate metabolic pathway

Glycogen is a glucose polymer stored in the liver, and the regulatory mechanism of glycogen metabolism is essential for blood glucose homeostasis. In my analysis, glycogen was identified as the WT mice-specific

5 increased metabolite, and unchanged glycogen could be one of the causes of hyperglycemia in *ob/ob* mice after glucose administration. As shown in Fig. 15, glycogen metabolism was the well-regulated pathway both by metabolite and by gene expression in both mice (Fig. 18). In WT mice, glucose-responsive molecules contributing to the increase of glycogen were pGs, pGp, glucan (1,4-alpha-), branching enzyme 1 (*Gbe1*), branching enzyme 1 (*Gbe1*), ectonucleotide pyrophosphatase/phosphodiesterase family member 3 (*Enpp3*),
10 G6P, ATP, UDP-glucose, and UMP. Among these glucose-responsive molecules, the WT mice-specific responses were the upregulation of *Gbe1*, the increase of ATP, the decrease of UMP. These responses could cause the dysfunction of glycogen storage and the followed hyperglycemia in *ob/ob* mice. The response of G6P also might contribute to WT mice-specific increase of glycogen, because the amplitude was quite larger in WT mice than in *ob/ob* mice (fold change at 60 min after glucose administration = 4.6, 1.4 in WT and *ob/ob* mice, respectively), although G6P was a common glucose-responsive metabolite.
15

The switching between glycolysis and gluconeogenesis is also indispensable mechanism for blood glucose homeostasis. Glycolysis is the degradative process of glucose to extract energy, and gluconeogenesis is the synthetic process of glucose to supply energy for other organs. Although the metabolic pathway was identified as the well-regulated pathway especially in WT mice (Fig. 15), the number of glucose-responsive molecules
20 contributing to *ob/ob* mice-specific hyperglycemia was limited; *Gck*, *G6pc*, Ala, and Ser (Fig. 19). This is partially because most of the reactions are common between glycolysis and gluconeogenesis. In WT mice, the gene encoding glucokinase (*Gck*) was strongly upregulated (fold change at 60 min = 3.5), and *G6pc* was strongly downregulated (fold change at 60 min = 0.39), both of which can account for the large increase of G6P (fold change at 60 min = 4.6). In contrast, both changes of gene expression were weaker in *ob/ob* mice
25 (fold change at 60 min = 1.1, 0.57, respectively), consistent with the small increase of G6P (fold change at 60

min = 1.4). The large increase of G6P directly activated glycolysis, and indirectly glycogen storage as shown above.

In fact, we identified the larger number of WT mice-specific inhibitory allosteric regulation of glycolysis. Especially, ATP, one of the products of glycolysis, was identified as the inhibitory allosteric regulator of three glycolytic metabolic reactions (Glucose to G6P, F6P to F1,6P, and PEP to pyruvate) in the WT mice network. This indicated the activation of glycolysis was accurately regulated through feedback system in healthy state.

In *ob/ob* mice, the increases of two amino acids, Ala and Ser, was identified as the inhibitory responses of one glycolytic reaction, PEP to pyruvate. By contrast, the decrease of citrate contributed to the activation of glycolysis, because the metabolite is an allosteric inhibitor of two glycolytic metabolic reactions (F6P to F1,6P, and pyruvate to acetyl CoA). In addition, some of enzyme genes such as glucose phosphate isomerase 1 (*Gpi*), aldolase A (*Aldoa*), *Gapdh*, and *Pklr* were upregulated specifically in *ob/ob* mice. Because most of them showed slow responses, these genes responded to the sustained hyperglycemia in the obese state.

3.9 The regulatory trans-omic network for glucose-responsive metabolic reactions in lipid metabolic pathway

Liver activates the synthesis of lipid to store energy after meals, and the excess lipid accumulation is one of the causes of insulin resistance (63). Trans-omic analysis of metabolic pathway showed that lipid pathway was more regulated by gene expressions than carbohydrate pathway (Fig. 15). Therefore, I analyzed the transcriptional regulation of lipid synthesis in the trans-omic networks (Fig. 20). In the genes in lipid synthesis, *Fasn* was upregulated in both WT and *ob/ob* mice, three genes were upregulated specifically in WT mice, such as long-chain acyl-CoA synthetases (*Acsl3* and *Acsl4*), and six genes were upregulated specifically in *ob/ob* mice, such as *Acacb*, *Gpd1*, *Gpat4*, and lipin 1 (*Lpin1*). *Egr1* were identified as the transcription factor regulating some of the *ob/ob* mice-specific glucose-responsive genes. In addition, increased taurocholate and phosphorylcholine (P-choline) allosterically activated metabolic reactions in lipid synthesis. These *ob/ob* mice-specific responses could enhanced lipid accumulation transcriptionally and allosterically in the obese state. By contrast, 5 out of 7 allosteric regulations by glucose-responsive metabolites, including increased ATP, inhibited

the metabolic reactions in lipid synthesis in WT mice, suggesting the prevention of lipid accumulation in the healthy state.

Cholesterol synthesis (terpenoid backbone biosynthesis and steroid biosynthesis) was transcriptionally activated pathway in WT mice (Fig. 15). Most of the genes in cholesterol synthesis were upregulated transiently (Fig. 21). *Srebf* was identified as the transcription factor regulating these glucose-responsive genes. Because cholesterol is made of acetyl CoA, some percentage of imported glucose could be converted into cholesterol altogether with glycolysis in the healthy state. On the other hand, 11 of 17 genes were downregulated in *ob/ob* mice, indicating the less production of cholesterol from glucose in the obese state.

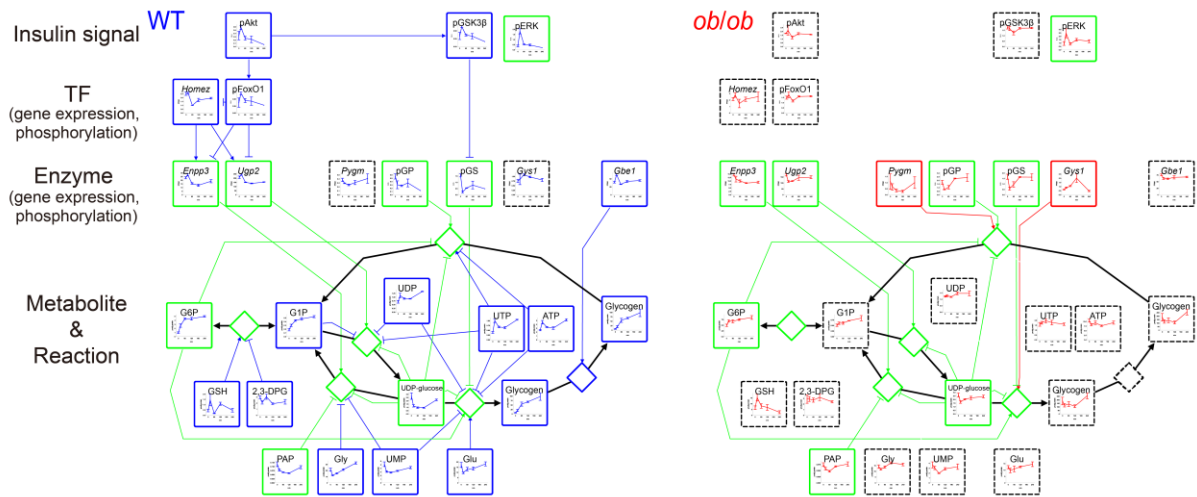
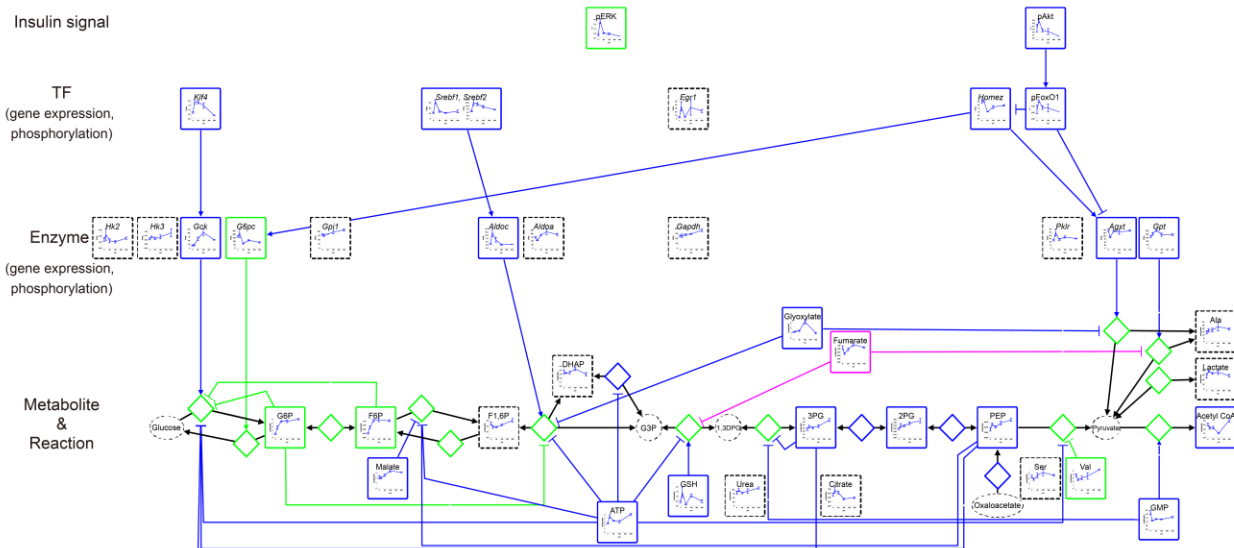


Figure 18. The regulatory trans-omic network for glucose-responsive metabolic reactions in glycogen metabolism.

The regulatory trans-omic network for glucose-responsive metabolic reactions in glycogen metabolism in the liver of WT mice and *ob/ob* mice. The information for glycogen metabolism was obtained from “starch and sucrose metabolism” (mmu00500) in the KEGG database (37, 38). Graphs of the time courses of measured molecules are shown for corresponding nodes as the means and SEMs of mice ($n = 5$ for metabolite, $n = 11$ or 12 for gene expression at 0 min, $n = 3$ for gene expression at 20 min, 60 min, 120 min, 240 min, $n = 3$ for phosphorylation). The colors of the frames indicate WT mice-specific glucose-responsive molecules (blue), *ob/ob* mice-specific glucose-responsive molecules (red), and common glucose-responsive molecules (green). The dashed frames indicate molecules that were not included in the glucose-responsive trans-omic network. Diamond nodes indicate metabolic reactions. The colored edges indicate inter-layer regulatory connections: WT mice-specific regulatory connections (blue), *ob/ob* mice-specific regulatory connections (red), and common inter-layer regulatory connections (green). From metabolite to reaction, only allosteric regulatory connections are colored. Black edges indicate the relationship between metabolic reactions and its substrate/product. The reversibility of metabolic reactions was obtained from the KEGG database (37, 38).

WT



ob/ob

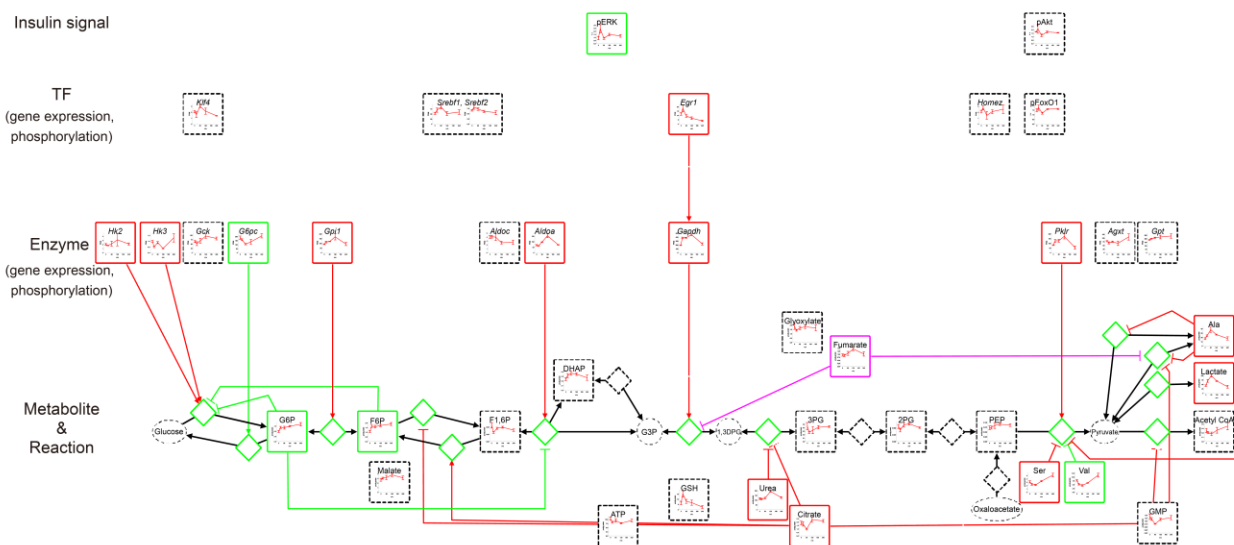


Figure 19. The regulatory trans-omic network for glucose-responsive metabolic reactions in glycolysis and gluconeogenesis.

The regulatory trans-omic network for glucose-responsive metabolic reactions in glycolysis and gluconeogenesis in the liver of WT mice and *ob/ob* mice. The information of glycolysis and gluconeogenesis were obtained from “glycolysis / gluconeogenesis” (mmu00010) in the KEGG database (37, 38). The glucose-responsive gene *Pgk1-rs7* is excluded. Graphs of the time courses of measured molecules are shown for corresponding nodes as the means and SEMs of mice (n = 5 for metabolite, n = 11 or 12 for gene expression at 0 min, n = 3 for gene expression at 20 min, 60 min, 120 min, 240 min, n = 3 for phosphorylation). The colors of the frames indicate WT mice-specific glucose-responsive molecules (blue), *ob/ob* mice-specific glucose-responsive molecules (red), common glucose-responsive molecules (green), and molecules showing opposite responses between WT mice and *ob/ob* mice (pink). The dashed frames indicate molecules that were not included in the glucose-responsive trans-omic network. Diamond nodes indicate metabolic reactions. The colored edges indicate inter-layer regulatory connections: WT mice-specific regulatory connections (blue), *ob/ob* mice-specific regulatory connections (red), common inter-layer regulatory connections (green), and opposite inter-layer regulatory connections (pink). From metabolite to reaction, only allosteric regulatory connections are colored. Black edges indicate the relationship between metabolic reactions and its substrate/product. The reversibility of metabolic reactions was obtained from the KEGG database (37, 38).

WT

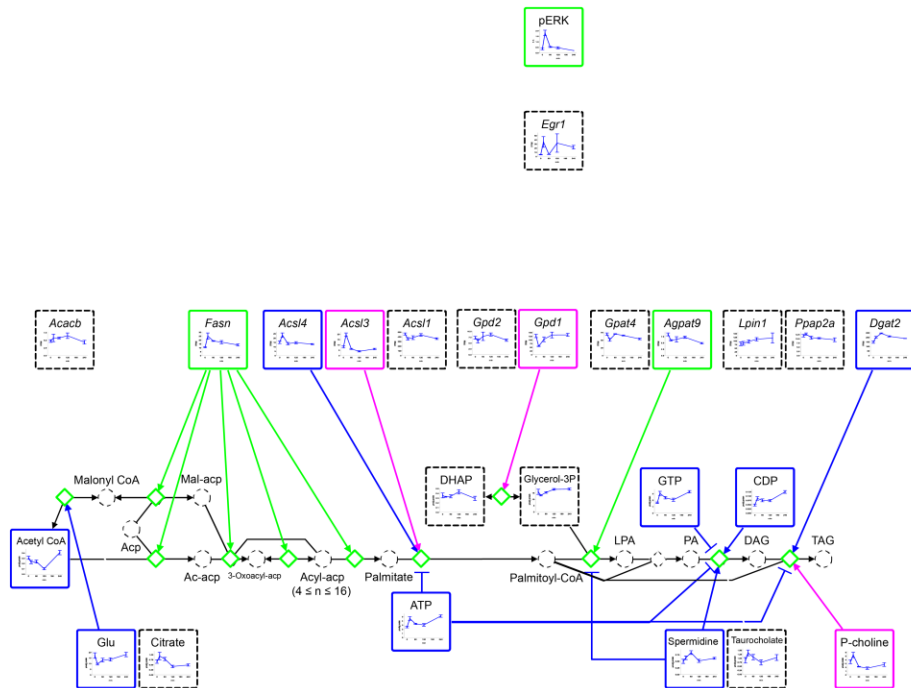
Insulin signal

TF

(gene expression,
phosphorylation)

Enzyme
(gene expression,
phosphorylation)

Metabolite
&
Reaction



oblob

Insulin signal

TF

(gene expression,
phosphorylation)

Enzyme
(gene expression,
phosphorylation)

Metabolite
&
Reaction

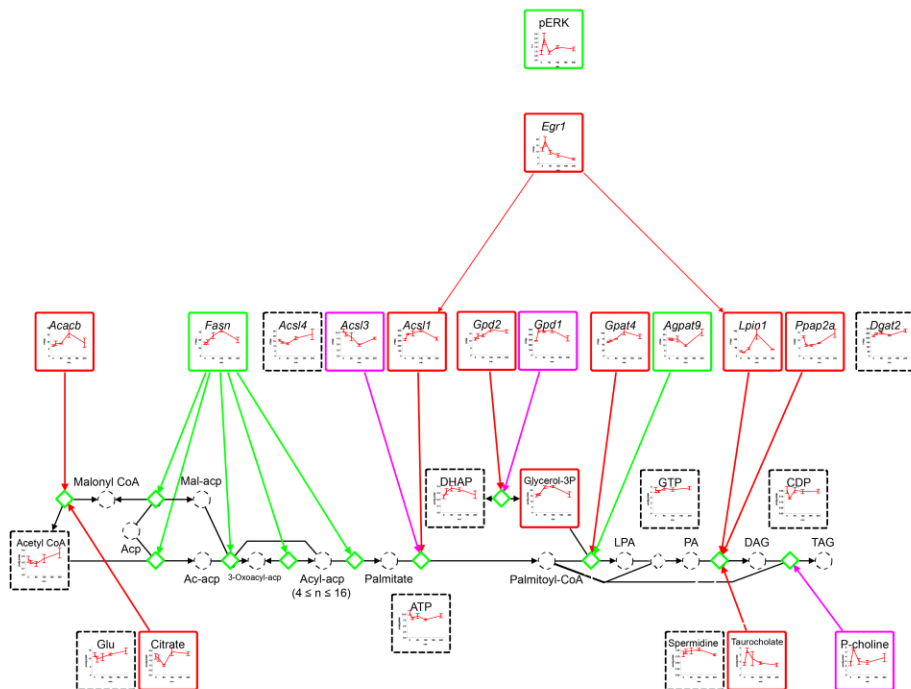


Figure 20. The regulatory trans-omic network for glucose-responsive metabolic reactions in lipid synthesis.

The regulatory trans-omic network for glucose-responsive metabolic reactions in lipid synthesis in the liver of WT mice and *ob/ob* mice. The information of lipid synthesis was obtained from “fatty acid biosynthesis” (mmu00061), “glycerolipid metabolism” (mmu00561), and “glycerophospholipid metabolism” (mmu00564) in the KEGG database (37, 38). Some intermediates in fatty acid biosynthesis are not plotted. Graphs of the time courses of measured molecules are shown for corresponding nodes as the means and SEMs of mice (n = 5 for metabolite, n = 11 or 12 for gene expression at 0 min, n = 3 for gene expression at 20 min, 60 min, 120 min, 240 min, n = 3 for phosphorylation). The colors of the frames indicate WT mice-specific glucose-responsive molecules (blue), *ob/ob* mice-specific glucose-responsive molecules (red), common glucose-responsive molecules (green), and molecules showing opposite responses between WT mice and *ob/ob* mice (pink). The dashed frames indicate molecules that were not included in the glucose-responsive trans-omic network. Diamond nodes indicate metabolic reactions. The colored edges indicate inter-layer regulatory connections: WT mice-specific regulatory connections (blue), *ob/ob* mice-specific regulatory connections (red), common inter-layer regulatory connections (green), and opposite inter-layer regulatory connections (pink). From metabolite to reaction, only allosteric regulatory connections are colored. Black edges indicate the relationship between metabolic reactions and its substrate/product. The reversibility of metabolic reactions was obtained from the KEGG database (37, 38).

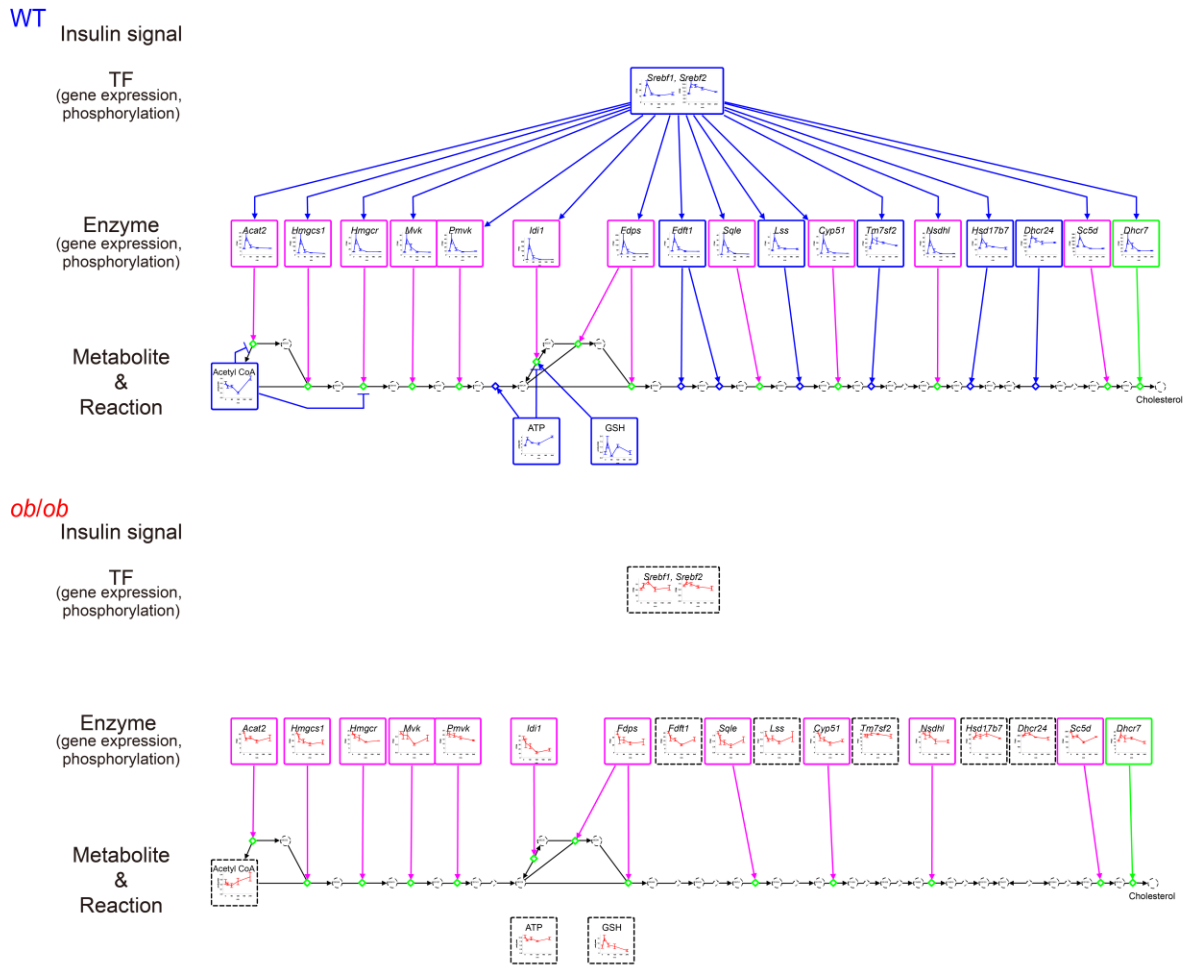


Figure 21. The regulatory trans-omic network for glucose-responsive metabolic reactions in cholesterol synthesis.

The regulatory trans-omic network for glucose-responsive metabolic reactions in cholesterol synthesis in the liver of WT mice and *ob/ob* mice. The information of cholesterol synthesis were obtained from “terpenoid backbone biosynthesis” (mmu00900) and “steroid biosynthesis” (mmu00100) in the KEGG database (37, 38). Graphs of the time courses of measured molecules are shown for corresponding nodes as the means and SEMs of mice (n = 5 for metabolite, n = 11 or 12 for gene expression at 0 min, n = 3 for gene expression at 20 min, 60 min, 120 min, 240 min, n = 3 for phosphorylation). The colors of the frames indicate WT mice-specific glucose-responsive molecules (blue), *ob/ob* mice-specific glucose-responsive molecules (red), common glucose-responsive molecules (green), and molecules showing opposite responses between WT mice and *ob/ob* mice (pink). The dashed frames indicate molecules that were not included in the glucose-responsive trans-omic network. Diamond nodes indicate metabolic reactions. The colored edges indicate inter-layer regulatory connections: WT mice-specific regulatory connections (blue), *ob/ob* mice-specific regulatory connections (red), common inter-layer regulatory connections (green), and opposite inter-layer regulatory connections (pink). From metabolite to reaction, only allosteric regulatory connections are colored. Black edges indicate the relationship between metabolic reactions and its substrate/product. The reversibility of metabolic reactions was obtained from the KEGG database (37, 38).

4. Discussion

4.1 Regulatory trans-omic network for glucose-responsive metabolic reactions in WT and *ob/ob* mice

In this study, I constructed regulatory trans-omic networks for glucose-responsive metabolic reactions in the liver of WT and *ob/ob* mice by integrating multi-omic data, and revealed global difference in regulation of glucose-responsive metabolic reactions between the liver of WT and *ob/ob* mice. In WT mice, a large part of metabolism was regulated by the rapid response of metabolites and by Akt-mediated genes of metabolic enzymes. Glucose-responsive metabolites, such as coenzymes ATP and NADP⁺, rapidly regulated many metabolic reactions in carbohydrate and amino acid metabolism, including the allosteric activation of glycogen synthesis and allosteric inhibition of glycolysis (Figs. 18 and 19). Akt was identified as the regulating signaling molecule of FoxO1 and FoxO1-mediated gene expression in WT mice. In addition, Akt might cause the upregulation of Srebf-mediated gene expression. A glucose-responsive gene *Srebf* was identified as the rapidly upregulated genes of metabolic enzymes in cholesterol synthesis (Fig. 21), which could induce the cholesterol esters synthesis and bile acids synthesis. This finding is consistent with the regulation of genes encoding metabolic enzymes related to cholesterol synthesis by Srebf (64). Because pAkt activates Srebf through mammalian target of rapamycin (mTor), and induces the expression of *Srebf* by autoregulation (65), the upregulation of *Srebf* might be caused by the glucose-responsive phosphorylation of Akt.

By contrast, in *ob/ob* mice, most of the rapid regulation of metabolic reactions by metabolites and those by *Srebf* was absent. Compensatorily, genes related to glycolysis, such as *Pklr* and *Gapdh*, and genes related to lipid synthesis, such as *Fasn* and *Acacb* were upregulated in the obese state (Figs. 19 and 20). I found that a glucose-responsive gene *Egr1* was the regulator of some of these upregulated genes. *Egr1* is one of the immediate early genes downstream of pErk (49, 50). Thus, *Egr1* was placed in the *ob/ob* network as a gene regulated by pErk. In addition, the slow upregulation of glucose-responsive genes in lipid synthesis may represent a mechanism of lipid accumulation in the liver of *ob/ob* mice. Consistently, de novo lipogenesis is promoted in the liver of insulin resistance (66). Because lipid accumulation is thought to be one of the causes of insulin resistance (63), the activation of lipid synthesis by the upregulated genes in *ob/ob* mice might be one

of the pathological mechanisms of lipid accumulation and insulin resistance in obesity. If the liver plays a major role of controlling postprandial blood glucose (8, 9), the rapid regulation of metabolic reactions in WT mice enables the transience of increased blood glucose after oral glucose administration, whereas the impairment of such rapid regulations and compensatory slow regulations in *ob/ob* mice cause sustained hyperglycemia (Fig. 3A).

4.2 Advantage of regulation of metabolic reaction by metabolite

The WT-specific regulation of metabolic reactions by glucose-responsive metabolites shows three unique advantages: speed, economy, and accuracy. Regulation of metabolic reactions by metabolites represents a form of direct control. Metabolites serve as allosteric regulators or substrates, without inducing other chemical reactions, such as protein phosphorylation and gene expression, saving the organism both time and energy. The control of metabolic reactions by metabolites directly affects the concentrations of the metabolites, enabling accurate regulation of metabolic reactions. By contrast, the regulation of metabolic reactions by changing the activity of the metabolic enzymes through changes in gene expression or protein phosphorylation are not directly controlled by metabolite concentrations. Therefore, controlling metabolic reactions through changes in gene expression is less precise than controlling the reactions through changes in metabolite concentrations. Thus, these analysis indicated that the response in WT mice is more rapid, less energy requiring, and more accurate than the response in obese mice. Technologies for large-scale identification of protein-metabolite interactions (67–69) will achieve the validation and further analysis of the regulation of metabolic reactions by metabolites.

4.3 Obese-specific upregulation of pErk-mediated gene expression

The trans-omic network analysis revealed that pAkt showed glucose-responsive phosphorylation specifically in the liver of WT mice, while pErk exhibited a common glucose-responsive increase in both WT and *ob/ob* mice. Previous observations demonstrated that insulin-induced phosphorylation of Erk is not affected by obesity and that of Akt decreases in obesity (70, 71). Although Erk showed common glucose-responsive

phosphorylation in both WT and *ob/ob* mice, the inter-layer regulatory connections from pErk to *Egr1* and the *Egr1*-mediated genes were identified only in *ob/ob* mice, but not in WT mice. The WT mice-specific activation of pErk-mediated gene expression might be caused by the shape of pErk responses. The phosphorylation of Erk in *ob/ob* mice was sustained, whereas the phosphorylation of Erk in WT mice was transient. Indeed, sustained phosphorylation of Erk, but not transient phosphorylation, induces downstream gene and protein expression of immediate early genes including *Egr1* (72, 73). Thus, the liver seems to conform to this paradigm of Erk signaling with sustained phosphorylation representing a key characteristic of the slow transcriptional response to glucose administration in the obese state.

4.4 Higher concentrations of carbohydrates in *ob/ob* mice

Some WT-specific glucose-responsive metabolites had higher concentrations in *ob/ob* mice than in WT mice. In *ob/ob* mice, such metabolites were not glucose-responsive, but were constantly maintained at higher concentrations, even after 16-h starvation. Thus, the metabolites constantly influenced metabolic reactions regardless of oral glucose administration in the obese state. The constantly increased metabolites included ATP, some metabolites in glycolysis and in the TCA cycle and pentose phosphate pathway, and reduced glutathione (Table 3), indicating constant high energy production and oxidation stress even during the fasting state in *ob/ob* mice. The absence of glucose-responsiveness of these metabolites in *ob/ob* mice may be caused by maximal energy production even during fasting state.

4.5 Comparison with previous studies

In this study, I focused on “glucose-responsiveness” of metabolite, gene expression, and protein phosphorylation after oral glucose administration in WT and *ob/ob* mice. The measurement of multi-omic time course data after oral glucose administration allowed us to identify glucose-responsive molecules in each layer, and inter-layer regulatory connections. The trans-omic networks is based on direct molecular interaction, rather than indirect statistical relationship (16). The same multi-omic data enable analysis of both the difference in

relative glucose-responsiveness of molecules and the difference in the amounts of molecules between WT and *ob/ob* mice, as shown in the last paragraph of each section of single-omic analysis.

Other studies have studied the difference in the amounts of molecules between healthy and obese mice using multi-omic data (14, 74, 75). However, none examined the difference of molecules between normal and obese mice in “glucose-responsiveness” after oral glucose administration as I did here. Soltis *et al.* (14) identified the epigenomic, transcriptomic, proteomic, and metabolomic differences between the liver of normal and high-fat diet (HFD)-induced obese mice in fasting state. Using network modeling approach based on interactome and computational methods, they identified differences in the amounts of molecules in multi-omic network between normal and obese mice. I found similar differences by analyzing my multi-omic data: Obese mice had increased carbohydrates, decreased lysophospholipids, upregulation of the metabolic enzyme genes in carbohydrate and lipid metabolism, and downregulation of the metabolic enzyme genes in amino acid metabolism. Here, the *ob/ob* mice were fed a normal diet, not a high-fat diet, thus the common differences between WT mice and the obese mice found in both studies are likely caused by obesity, rather than by the content of diets or by the lack of leptin in the *ob/ob* mice. In addition, diet-induced obese mice show leptin resistance and dysregulation of hepatic metabolic response similar to *ob/ob* mice (76, 77).

4.6 Future work

To construct the regulatory trans-omic networks for glucose-responsive metabolic reactions, I used transcriptomic and metabolomic data and data of selected signaling proteins measured by Western blotting.

Because of the lower comprehensiveness of the data measured by Western blotting compared to the transcriptomic and metabolomic data, the numbers of signaling molecules, transcription factors and their inter-layer regulatory connections in the trans-omic network were much poorer than those of metabolites, gene expression and their inter-layer regulatory connections. In particular, most of the glucose-responsive genes encoding metabolic enzymes was not connected to their transcription factors in the *ob/ob* mice network.

Proteomic data (78, 79) and phosphoproteomic data (15, 18, 80) will provide large-scale information about the regulation of metabolic reactions by changes in the amount and phosphorylation of transcription factors and

metabolic enzymes. In addition, detailed information about the binding affinities between metabolic enzymes and metabolites are required for a comprehensive identification of the regulation of metabolism by glucose-responsive metabolites. Epigenomic data, including histone modification and DNA methylation, will reveal regulatory mechanisms controlling of glucose-responsive genes (81–84). Because some metabolites in the liver are regulated by transport between blood and liver, the regulation of such metabolites between blood and liver requires consideration of the transporters that control the distribution of these metabolites (85, 86). Although this trans-omic network is not comprehensive, I used the network to reveal key insights into how liver metabolism is differentially regulated between the healthy and obese states in response to glucose. This in vivo study provides key insights into how obesity profoundly changes the regulatory profile, shifting regulation away from rapid regulation by metabolites to slow regulation by gene expression.

5. References

1. Action to Control Cardiovascular Risk in Diabetes Study Group, H. C. Gerstein, M. E. Miller, R. P. Byington, D. C. Goff, J. T. Bigger, J. B. Buse, W. C. Cushman, S. Genuth, F. Ismail-Beigi, R. H. Grimm, J. L. Probstfield, D. G. Simons-Morton, W. T. Friedewald, Effects of intensive glucose lowering in type 2 diabetes. *N. Engl. J. Med.* **358**, 2545–59 (2008).
2. Diabetes Control and Complications Trial Research Group, D. M. Nathan, S. Genuth, J. Lachin, P. Cleary, O. Crofford, M. Davis, L. Rand, C. Siebert, The effect of intensive treatment of diabetes on the development and progression of long-term complications in insulin-dependent diabetes mellitus. *N. Engl. J. Med.* **329**, 977–86 (1993).
3. ADVANCE Collaborative Group, A. Patel, S. MacMahon, J. Chalmers, B. Neal, L. Billot, M. Woodward, M. Marre, M. Cooper, P. Glasziou, D. Grobbee, P. Hamet, S. Harrap, S. Heller, L. Liu, G. Mancia, C. E. Mogensen, C. Pan, N. Poulter, A. Rodgers, B. Williams, S. Bompaint, B. E. de Galan, R. Joshi, F. Travert, Intensive blood glucose control and vascular outcomes in patients with type 2 diabetes. *N. Engl. J. Med.* **358**, 2560–72 (2008).
4. G. F. Cahill, Fuel metabolism in starvation. *Annu. Rev. Nutr.* **26**, 1–22 (2006).
5. S. E. Kahn, R. L. Hull, K. M. Utzschneider, Mechanisms linking obesity to insulin resistance and type 2 diabetes. *Nature*. **444**, 840–6 (2006).
6. S. V.T., S. G.I., The pathogenesis of insulin resistance: Integrating signaling pathways and substrate flux. *J. Clin. Invest.* **126**, 12–22 (2016).
7. M. C. Petersen, D. F. Vatner, G. I. Shulman, Regulation of hepatic glucose metabolism in health and disease. *Nat. Rev. Endocrinol.* **13**, 572–587 (2017).
8. J. Radziuk, S. Pye, Hepatic glucose uptake, gluconeogenesis and the regulation of glycogen synthesis. *Diabetes. Metab. Res. Rev.* **17**, 250–72 (2001).
9. A. D. Cherrington, Banting Lecture 1997. Control of glucose uptake and release by the liver in vivo. *Diabetes*. **48**, 1198–214 (1999).

10. E. A. Franzosa, T. Hsu, A. Sirota-Madi, A. Shafquat, G. Abu-Ali, X. C. Morgan, C. Huttenhower, Sequencing and beyond: Integrating molecular “omics” for microbial community profiling. *Nat. Rev. Microbiol.* **13**, 360–372 (2015).
11. Y. Hasin, M. Seldin, A. Lusi, Multi-omics approaches to disease. *Genome Biol.* **18**, 1–15 (2017).
12. L. Gerosa, B. R. B. Haverkorn van Rijsewijk, D. Christodoulou, K. Kochanowski, T. S. B. Schmidt, E. Noor, U. Sauer, Pseudo-transition Analysis Identifies the Key Regulators of Dynamic Metabolic Adaptations from Steady-State Data. *Cell Syst.* **1**, 270–282 (2015).
13. S. R. Hackett, V. R. T. Zanolli, W. Xu, J. Goya, J. O. Park, D. H. Perlman, P. A. Gibney, D. Botstein, J. D. Storey, J. D. Rabinowitz, Systems-level analysis of mechanisms regulating yeast metabolic flux. *Science.* **354** (2016), doi:10.1126/science.aaf2786.
14. A. R. Soltis, N. J. Kennedy, X. Xin, F. Zhou, S. B. Ficarro, Y. S. Yap, B. J. Matthews, D. A. Lauffenburger, F. M. White, J. A. Marto, R. J. Davis, E. Fraenkel, Hepatic Dysfunction Caused by Consumption of a High-Fat Diet. *Cell Rep.* **21**, 3317–3328 (2017).
15. K. Yugi, H. Kubota, Y. Toyoshima, R. Noguchi, K. Kawata, Y. Komori, S. Uda, K. Kunida, Y. Tomizawa, Y. Funato, H. Miki, M. Matsumoto, K. I. Nakayama, K. Kashikura, K. Endo, K. Ikeda, T. Soga, S. Kuroda, Reconstruction of Insulin Signal Flow from Phosphoproteome and Metabolome Data. *Cell Rep.* **8**, 1171–1183 (2014).
16. K. Yugi, H. Kubota, A. Hatano, S. Kuroda, Trans-Omics: How To Reconstruct Biochemical Networks Across Multiple “Omic” Layers. *Trends Biotechnol.* **34**, 276–290 (2016).
17. K. Yugi, S. Kuroda, Metabolism-Centric Trans-Omics. *Cell Syst.* **4**, 19–20 (2017).
18. K. Kawata, A. Hatano, K. Yugi, H. Kubota, T. Sano, M. Fujii, Y. Tomizawa, T. Kokaji, K. Y. Tanaka, S. Uda, Y. Suzuki, M. Matsumoto, K. I. Nakayama, K. Saitoh, K. Kato, A. Ueno, M. Ohishi, A. Hirayama, T. Soga, S. Kuroda, Trans-omic Analysis Reveals Selective Responses to Induced and Basal Insulin across Signaling, Transcriptional, and Metabolic Networks. *iScience.* **7**, 212–229 (2018).
19. P. Lindström, The physiology of obese-hyperglycemic mice [ob/ob mice]. *ScientificWorldJournal.* **7**, 666–85 (2007).
20. T. Soga, D. N. Heiger, Amino acid analysis by capillary electrophoresis electrospray ionization mass spectrometry. *Anal. Chem.* **72**, 1236–41 (2000).

21. T. Soga, R. Baran, M. Suematsu, Y. Ueno, S. Ikeda, T. Sakurakawa, Y. Kakazu, T. Ishikawa, M. Robert, T. Nishioka, M. Tomita, Differential metabolomics reveals ophthalmic acid as an oxidative stress biomarker indicating hepatic glutathione consumption. *J. Biol. Chem.* **281**, 16768–16776 (2006).
22. T. Soga, K. Igarashi, C. Ito, K. Mizobuchi, H.-P. Zimmermann, M. Tomita, Metabolomic profiling of anionic metabolites by capillary electrophoresis mass spectrometry. *Anal. Chem.* **81**, 6165–74 (2009).
23. N. Ishii, K. Nakahigashi, T. Baba, M. Robert, T. Soga, A. Kanai, T. Hirasawa, M. Naba, K. Hirai, A. Hoque, P. Y. Ho, Y. Kakazu, K. Sugawara, S. Igarashi, S. Harada, T. Masuda, N. Sugiyama, T. Togashi, M. Hasegawa, Y. Takai, K. Yugi, K. Arakawa, N. Iwata, Y. Toya, Y. Nakayama, T. Nishioka, K. Shimizu, H. Mori, M. Tomita, Multiple high-throughput analyses monitor the response of *E. coli* to perturbations. *Science*. **316**, 593–7 (2007).
24. K. Ikeda, in *Bioactive Lipid Mediators* (Springer Japan, Tokyo, 2015; http://link.springer.com/10.1007/978-4-431-55669-5_25), pp. 349–356.
25. H. Tsugawa, K. Ikeda, W. Tanaka, Y. Senoo, M. Arita, M. Arita, Comprehensive identification of sphingolipid species by in silico retention time and tandem mass spectral library. *J. Cheminform.* **9**, 19 (2017).
26. R. Noguchi, H. Kubota, K. Yugi, Y. Toyoshima, Y. Komori, T. Soga, S. Kuroda, The selective control of glycolysis, gluconeogenesis and glycogenesis by temporal insulin patterns. *Mol. Syst. Biol.* **9**, 664 (2013).
27. A. Von Wilamowitz-Moellendorff, R. W. Hunter, M. García-Rocha, L. Kang, I. López-Soldado, L. Lantier, K. Patel, M. W. Pegg, C. Martínez-Pons, M. Voss, J. Calbó, P. T. W. Cohen, D. H. Wasserman, J. J. Guinovart, K. Sakamoto, Glucose-6-phosphate-mediated activation of liver glycogen synthase plays a key role in hepatic glycogen synthesis. *Diabetes*. **62**, 4070–4082 (2013).
28. K. Matsumoto, A. Suzuki, H. Wakaguri, S. Sugano, Y. Suzuki, Construction of mate pair full-length cDNAs libraries and characterization of transcriptional start sites and termination sites. *Nucleic Acids Res.* **42** (2014), doi:10.1093/nar/gku600.
29. P. Flicek, M. R. Amodé, D. Barrell, K. Beal, K. Billis, S. Brent, D. Carvalho-Silva, P. Clapham, G. Coates, S. Fitzgerald, L. Gil, C. G. Girón, L. Gordon, T. Hourlier, S. Hunt, N. Johnson, T. Juettemann, A. K. Kähäri, S. Keenan, E. Kulesha, F. J. Martin, T. Maurel, W. M. McLaren, D. N. Murphy, R. Nag, B. Overduin, M. Pignatelli, B. Pritchard, E. Pritchard, H. S. Riat, M. Ruffier, D. Sheppard, K. Taylor, A. Thormann, S. J.

- Trevanion, A. Vullo, S. P. Wilder, M. Wilson, A. Zadissa, B. L. Aken, E. Birney, F. Cunningham, J. Harrow, J. Herrero, T. J. P. Hubbard, R. Kinsella, M. Muffato, A. Parker, G. Spudich, A. Yates, D. R. Zerbino, S. M. J. Searle, Ensembl 2014. *Nucleic Acids Res.* **42**, 749–755 (2014).
30. F. Cunningham, M. R. Amode, D. Barrell, K. Beal, K. Billis, S. Brent, D. Carvalho-Silva, P. Clapham, G. Coates, S. Fitzgerald, L. Gil, C. G. Girón, L. Gordon, T. Hourlier, S. E. Hunt, S. H. Janacek, N. Johnson, T. Juettemann, A. K. Kähäri, S. Keenan, F. J. Martin, T. Maurel, W. McLaren, D. N. Murphy, R. Nag, B. Overduin, A. Parker, M. Patricio, E. Perry, M. Pignatelli, H. S. Riat, D. Sheppard, K. Taylor, A. Thormann, A. Vullo, S. P. Wilder, A. Zadissa, B. L. Aken, E. Birney, J. Harrow, R. Kinsella, M. Muffato, M. Ruffier, S. M. J. Searle, G. Spudich, S. J. Trevanion, A. Yates, D. R. Zerbino, P. Flicek, Ensembl 2015. *Nucleic Acids Res.* **43**, D662–D669 (2015).
 31. C. Trapnell, A. Roberts, L. Goff, G. Pertea, D. Kim, D. R. Kelley, H. Pimentel, S. L. Salzberg, J. L. Rinn, L. Pachter, Differential gene and transcript expression analysis of RNA-seq experiments with TopHat and Cufflinks. *Nat. Protoc.* **7**, 562–578 (2012).
 32. C. Trapnell, L. Pachter, S. L. Salzberg, TopHat: Discovering splice junctions with RNA-Seq. *Bioinformatics.* **25**, 1105–1111 (2009).
 33. T. Sano, K. Kawata, S. Ohno, K. Yugi, H. Kakuda, H. Kubota, S. Uda, M. Fujii, K. Kunida, D. Hoshino, A. Hatano, Y. Ito, M. Sato, Y. Suzuki, S. Kuroda, Selective control of up-regulated and down-regulated genes by temporal patterns and doses of insulin. *Sci. Signal.* **9**, ra112 (2016).
 34. C. Trapnell, B. A. Williams, G. Pertea, A. Mortazavi, G. Kwan, M. J. Van Baren, S. L. Salzberg, B. J. Wold, L. Pachter, Transcript assembly and quantification by RNA-Seq reveals unannotated transcripts and isoform switching during cell differentiation. *Nat. Biotechnol.* **28**, 511–515 (2010).
 35. J. D. Storey, A direct approach to false discovery rates. *J. R. Stat. Soc. Ser. B Stat. Methodol.* (2002).
 36. Y. H. Yoav Benjamini, Controlling the False Discovery Rate : A Practical and Powerful Approach to Multiple Testing. *J. R. Stastical Soc.* **57**, 289–300 (1995).
 37. M. Kanehisa, S. Goto, Y. Sato, M. Furumichi, M. Tanabe, KEGG for integration and interpretation of large-scale molecular data sets. *Nucleic Acids Res.* **40**, 109–114 (2012).
 38. M. Kanehisa, M. Furumichi, M. Tanabe, Y. Sato, K. Morishima, KEGG: New perspectives on genomes, pathways, diseases and drugs. *Nucleic Acids Res.* **45**, D353–D361 (2017).

39. R. J. Kinsella, A. Kähäri, S. Haider, J. Zamora, G. Proctor, G. Spudich, J. Almeida-King, D. Staines, P. Derwent, A. Kerhornou, P. Kersey, P. Flicek, Ensembl BioMarts: A hub for data retrieval across taxonomic space. *Database*. **2011**, 1–9 (2011).
40. E. Arner, C. O. Daub, K. Vitting-Seerup, R. Andersson, B. Lilje, F. Drabløs, A. Lennartsson, M. Rönnerblad, O. Hrydziuszko, M. Vitezic, T. C. Freeman, A. M. N. Alhendi, P. Arner, R. Axton, J. K. Baillie, A. Beckhouse, B. Bodega, J. Briggs, F. Brombacher, M. Davis, M. Detmar, A. Ehrlund, M. Endoh, A. Eslami, M. Fagiolini, L. Fairbairn, G. J. Faulkner, C. Ferrai, M. E. Fisher, L. Forrester, D. Goldowitz, R. Guler, T. Ha, M. Hara, M. Herlyn, T. Ikawa, C. Kai, H. Kawamoto, L. M. Khachigian, S. P. Klinken, S. Kojima, H. Koseki, S. Klein, N. Mejhert, K. Miyaguchi, Y. Mizuno, M. Morimoto, K. J. Morris, C. Mummery, Y. Nakachi, S. Ogishima, M. Okada-Hatakeyama, Y. Okazaki, V. Orlando, D. Ovchinnikov, R. Passier, M. Patrikakis, A. Pombo, X.-Y. Qin, S. Roy, H. Sato, S. Savvi, A. Saxena, A. Schwegmann, D. Sugiyama, R. Swoboda, H. Tanaka, A. Tomoiu, L. N. Winteringham, E. Wolvetang, C. Yanagi-Mizuochi, M. Yoneda, S. Zabierowski, P. Zhang, I. Abugessaisa, N. Bertin, A. D. Diehl, S. Fukuda, M. Furuno, J. Harshbarger, A. Hasegawa, F. Hori, S. Ishikawa-Kato, Y. Ishizu, M. Itoh, T. Kawashima, M. Kojima, N. Kondo, M. Lizio, T. F. Meehan, C. J. Mungall, M. Murata, H. Nishiyori-Sueki, S. Sahin, S. Nagao-Sato, J. Severin, M. J. L. de Hoon, J. Kawai, T. Kasukawa, T. Lassmann, H. Suzuki, H. Kawaji, K. M. Summers, C. Wells, FANTOM Consortium, D. A. Hume, A. R. R. Forrest, A. Sandelin, P. Carninci, Y. Hayashizaki, Transcribed enhancers lead waves of coordinated transcription in transitioning mammalian cells. *Science*. **347**, 1010–4 (2015).
41. V. Matys, O. V. Kel-Margoulis, E. Fricke, I. Liebich, S. Land, A. Barre-Dirrie, I. Reuter, D. Chekmenev, M. Krull, K. Hornischer, N. Voss, P. Stegmaier, B. Lewicki-Potapov, H. Saxel, A. E. Kel, E. Wingender, TRANSFAC(R) and its module TRANSCOMP(R): transcriptional gene regulation in eukaryotes. *Nucl. Acids Res.* **34**, D108–110 (2006).
42. A. E. Kel, E. Gößling, I. Reuter, E. Cheremushkin, O. V. Kel-Margoulis, E. Wingender, MATCHTM: A tool for searching transcription factor binding sites in DNA sequences. *Nucleic Acids Res.* **31**, 3576–3579 (2003).
43. L. Rui, Energy metabolism in the liver. *Compr. Physiol.* **4**, 177–97 (2014).

44. S. Oki, T. Ohta, G. Shioi, H. Hatanaka, O. Ogasawara, Y. Okuda, H. Kawaji, R. Nakaki, J. Sese, C. Meno, ChIP-Atlas: a data-mining suite powered by full integration of public ChIP-seq data. *EMBO Rep.* **19**, e46255 (2018).
45. I. Schomburg, A. Chang, S. Placzek, C. Söhngen, M. Rother, M. Lang, C. Munaretto, S. Ulas, M. Stelzer, A. Grote, M. Scheer, D. Schomburg, BRENDA in 2013: Integrated reactions, kinetic data, enzyme function data, improved disease classification: New options and contents in BRENDA. *Nucleic Acids Res.* **41**, 764–772 (2013).
46. C. J. Bult, J. T. Eppig, J. A. Kadin, J. E. Richardson, J. A. Blake, Mouse Genome Database Group, The Mouse Genome Database (MGD): mouse biology and model systems. *Nucleic Acids Res.* **36**, D724-8 (2008).
47. J. Nakae, T. Kitamura, D. L. Silver, D. Accili, The forkhead transcription factor Foxo1 (Fkhr) confers insulin sensitivity onto glucose-6- phosphatase expression. *J. Clin. invest.* **111**, 1359–1367 (2001).
48. A. Barthel, D. Schmoll, T. G. Unterman, FoxO proteins in insulin action and metabolism. *Trends Endocrinol. Metab.* **16**, 183–189 (2005).
49. D. Gineitis, R. Treisman, Differential Usage of Signal Transduction Pathways Defines Two Types of Serum Response Factor Target Gene. *J. Biol. Chem.* **276**, 24531–24539 (2001).
50. T. Harada, T. Morooka, S. Ogawa, E. Nishida, ERK induces p35, a neuron-specific activator of Cdk5, through induction of Egr1. *Nat. Cell Biol.* **3**, 453–459 (2001).
51. K. R. Albe, M. H. Butler, B. E. Wright, Cellular concentrations of enzymes and their substrates. *J. Theor. Biol.* **143**, 163–195 (1990).
52. R. Milo, What is the total number of protein molecules per cell volume? A call to rethink some published values. *BioEssays.* **35**, 1050–1055 (2013).
53. B. H. Junker, C. Klukas, F. Schreiber, Vanted: A system for advanced data analysis and visualization in the context of biological networks. *BMC Bioinformatics.* **7**, 1–13 (2006).
54. T. Kokaji, A. Hatano, Y. Ito, K. Yugi, M. Eto, S. Ohno, M. Fujii, K. Hironaka, R. Egami, H. Inoue, S. Uda, H. Kubota, Y. Suzuki, K. Ikeda, M. Arita, M. Matsumoto, K. I. Nakayama, A. Hirayama, T. Soga, S. Kuroda, Trans-omic analysis reveals allosteric and gene regulation-axes for altered glucose-responsive liver metabolism associated with obesity. *bioRxiv*, 653758 (2019).

55. G. Perriello, R. Jorde, N. Nurjhan, M. Stumvoll, G. Dailey, T. Jenssen, D. M. Bier, J. E. Gerich, Estimation of glucose-alanine-lactate-glutamine cycles in postabsorptive humans: role of skeletal muscle. *Am. J. Physiol.* **269**, E443-50 (1995).
56. J. Katz, J. a Tayek, Gluconeogenesis and the Cori cycle in 12-, 20-, and 40-h-fasted humans. *Am. J. Physiol.* **275**, E537–E542 (1998).
57. M. a Herman, B. B. Kahn, Glucose transport and sensing in the maintenance of glucose homeostasis and metabolic harmony. *J. Clin. Invest.* **116**, 1767–75 (2006).
58. O. Shaham, R. Wei, T. J. Wang, C. Ricciardi, G. D. Lewis, R. S. Vasan, S. a Carr, R. Thadhani, R. E. Gerszten, V. K. Mootha, Metabolic profiling of the human response to a glucose challenge reveals distinct axes of insulin sensitivity. *Mol. Syst. Biol.* **4**, 214 (2008).
59. Y. Shimomura, T. Honda, M. Shiraki, T. Murakami, J. Sato, H. Kobayashi, K. Mawatari, M. Obayashi, R. A. Harris, Branched-chain amino acid catabolism in exercise and liver disease. *J. Nutr.* **136**, 250S–3S (2006).
60. L. Laffel, Ketone bodies: a review of physiology, pathophysiology and application of monitoring to diabetes. *Diabetes. Metab. Res. Rev.* **15**, 412–426 (1999).
61. R. C. Nordlie, J. D. Foster, A. J. Lange, Regulation of glucose production by the liver. *Annu. Rev. Nutr.* **19**, 379–406 (1999).
62. J. O. Park, S. A. Rubin, Y.-F. Xu, D. Amador-Noguez, J. Fan, T. Shlomi, J. D. Rabinowitz, Metabolite concentrations, fluxes and free energies imply efficient enzyme usage. *Nat. Chem. Biol.* **12**, 482–9 (2016).
63. V. T. Samuel, G. I. Shulman, Mechanisms for insulin resistance: common threads and missing links. *Cell.* **148**, 852–71 (2012).
64. J. D. Horton, J. L. Goldstein, M. S. Brown, SREBPs: activators of the complete program of cholesterol and fatty acid synthesis in the liver. *J. Clin. Invest.* **109**, 1125–31 (2002).
65. T. Il Jeon, T. F. Osborne, SREBPs: Metabolic integrators in physiology and metabolism. *Trends Endocrinol. Metab.* **23**, 65–72 (2012).
66. M. Roden, Mechanisms of Disease: Hepatic steatosis in type 2 diabetes - Pathogenesis and clinical relevance. *Nat. Clin. Pract. Endocrinol. Metab.* **2**, 335–348 (2006).

67. G. X. Yang, X. Li, M. Snyder, Investigating metabolite-protein interactions: An overview of available techniques. *Methods*. **57**, 459–466 (2012).
68. M. Diether, U. Sauer, Towards detecting regulatory protein–metabolite interactions. *Curr. Opin. Microbiol.* **39**, 16–23 (2017).
69. I. Piazza, K. Kochanowski, V. Cappelletti, T. Fuhrer, E. Noor, U. Sauer, P. Picotti, A Map of Protein-Metabolite Interactions Reveals Principles of Chemical Communication. *Cell*. **172**, 358–372.e23 (2018).
70. Z. Y. Jiang, Y. W. Lin, A. Clemont, E. P. Feener, K. D. Hein, M. Igarashi, T. Yamauchi, M. F. White, G. L. King, Characterization of selective resistance to insulin signaling in the vasculature of obese Zucker (fa/fa) rats. *J. Clin. Invest.* **104**, 447–57 (1999).
71. K. Cusi, K. Maezono, A. Osman, M. Pendergrass, M. E. Patti, T. Pratipanawatr, R. A. DeFronzo, C. R. Kahn, L. J. Mandarino, Insulin resistance differentially affects the PI 3-kinase- and MAP kinase-mediated signaling in human muscle. *J. Clin. Invest.* **105**, 311–20 (2000).
72. L. O. Murphy, J. P. MacKeigan, J. Blenis, A network of immediate early gene products propagates subtle differences in mitogen-activated protein kinase signal amplitude and duration. *Mol. Cell. Biol.* **24**, 144–53 (2004).
73. M. Ebisuya, The duration, magnitude and compartmentalization of ERK MAP kinase activity: mechanisms for providing signaling specificity. *J. Cell Sci.* **118**, 2997–3002 (2005).
74. B. W. Parks, T. Sallam, M. Mehrabian, N. Psychogios, S. T. Hui, F. Norheim, L. W. Castellani, C. D. Rau, C. Pan, J. Phun, Z. Zhou, W. P. Yang, I. Neuhaus, P. S. Gargalovic, T. G. Kirchgesner, M. Graham, R. Lee, P. Tontonoz, R. E. Gerszten, A. L. Hevener, A. J. Lusis, Genetic architecture of insulin resistance in the mouse. *Cell Metab.* **21**, 334–346 (2015).
75. E. G. Williams, Y. Wu, P. Jha, S. Dubuis, P. Blattmann, C. A. Argmann, S. M. Houten, T. Amariuta, W. Wolski, N. Zamboni, R. Aebersold, J. Auwerx, Systems proteomics of liver mitochondria function. *Science*. **352**, aad0189 (2016).
76. N. Sáinz, J. Barrenetxe, M. J. Moreno-Aliaga, J. A. Martínez, Leptin resistance and diet-induced obesity: central and peripheral actions of leptin. *Metabolism*. **64**, 35–46 (2015).
77. P. J. Scarpace, Y. Zhang, Leptin resistance: a predisposing factor for diet-induced obesity. *Am. J. Physiol. Integr. Comp. Physiol.* **296**, R493–R500 (2009).

78. B. Schwanhäusser, D. Busse, N. Li, G. Dittmar, J. Schuchhardt, J. Wolf, W. Chen, M. Selbach, Global quantification of mammalian gene expression control. *Nature*. **473**, 337–342 (2011).
79. A. R. Kristensen, J. Gsponer, L. J. Foster, Protein synthesis rate is the predominant regulator of protein expression during differentiation. *Mol. Syst. Biol.* **9**, 689 (2013).
80. S. J. Humphrey, G. Yang, P. Yang, D. J. Fazakerley, J. Stöckli, J. Y. Yang, D. E. James, Dynamic adipocyte phosphoproteome reveals that Akt directly regulates mTORC2. *Cell Metab.* **17**, 1009–20 (2013).
81. M. Ahrens, O. Ammerpohl, W. Von Schönfels, J. Kolarova, S. Bens, T. Itzel, A. Teufel, A. Herrmann, M. Brosch, H. Hinrichsen, W. Erhart, J. Egberts, B. Sipos, S. Schreiber, R. Häsler, F. Stickel, T. Becker, M. Krawczak, C. Röcken, R. Siebert, C. Schafmayer, J. Hampe, DNA methylation analysis in nonalcoholic fatty liver disease suggests distinct disease-specific and remodeling signatures after bariatric surgery. *Cell Metab.* **18**, 296–302 (2013).
82. H. Kirchner, I. Sinha, H. Gao, M. A. Ruby, M. Schönke, J. M. Lindvall, R. Barrès, A. Krook, E. Näslund, K. Dahlman-Wright, J. R. Zierath, Altered DNA methylation of glycolytic and lipogenic genes in liver from obese and type 2 diabetic patients. *Mol. Metab.* **5**, 171–183 (2016).
83. J. Lee, Y. Kim, S. Friso, S. W. Choi, Epigenetics in non-alcoholic fatty liver disease. *Mol. Aspects Med.* **54**, 78–88 (2017).
84. C. Ling, T. Rönn, Epigenetics in Human Obesity and Type 2 Diabetes. *Cell Metab.* **29**, 1028–1044 (2019).
85. A. Noronha, J. Modamio, Y. Jarosz, E. Guerard, N. Sompairac, G. Preciat, A. D. Daníelsdóttir, M. Krecke, D. Merten, H. S. Haraldsdóttir, A. Heinken, L. Heirendt, S. Magnúsdóttir, D. A. Ravcheev, S. Sahoo, P. Gawron, L. Friscioni, B. Garcia, M. Prendergast, A. Puente, M. Rodrigues, A. Roy, M. Rouquaya, L. Wiltgen, A. Žagare, E. John, M. Krueger, I. Kuperstein, A. Zinovyev, R. Schneider, R. M. T. Fleming, I. Thiele, The Virtual Metabolic Human database: integrating human and gut microbiome metabolism with nutrition and disease. *Nucleic Acids Res.* **47**, D614–D624 (2019).
86. M. I. Sigurdsson, N. Jamshidi, E. Steingrímsson, I. Thiele, B. T. Palsson, A detailed genome-wide reconstruction of mouse metabolism based on human Recon 1. *BMC Syst. Biol.* **4** (2010), doi:10.1186/1752-0509-4-140.

6. Acknowledgments

I thank my supervisor, Professor Shinya Kuroda, for teaching principles as a scientific researcher. I thank Ms. Yuki Ito for her effort on experiment and sequence analysis. I thank Dr. Hatano Atsushi for his effort on experiment. I thank Professor Hiroyuki Kubota, Dr. Shinsuke Uda, and Dr. Katsuyuki Yugi for his advice on experimental technique of mice, statistical method and idea, and bioinformatic analysis. I thank for Professor Tomonori Soga, Dr. Akiyoshi Hirayama, Professor Makoto Arita, Dr. Kazutaka Ikeda, and Professor Yutaka Suzuki for performing each type of omics measurement. I thank for Professor Hiroshi Inoue, Dr. Fumio Matsuda, Dr. Miki Eto, Dr. Satoshi Ohno, Dr. Masashi Fujii, Dr. Ken-ichi Hironaka, Dr. Takaho Tsuchiya, Dr. Kentaro Kawata, Dr. Takanori Sano, Dr. Takamasa Kudo, Mr. Riku Egami, and all the Kuroda Laboratory members for their advice, discussion and suggestions. The computational analysis of this work was performed in part with support of the super computer system of National Institute of Genetics (NIG), Research Organization of Information and Systems (ROIS). Sequencing data measured in this study have been deposited in the DNA Data Bank of Japan Sequence Read Archive (DRA) (www.ddbj.nig.ac.jp/) under the accession no. DRA008416.

This work was supported by the Creation of Fundamental Technologies for Understanding and Control of Biosystem Dynamics, CREST (JPMJCR12W3) from the Japan Science and Technology Agency (JST) and by the Japan Society for the Promotion of Science (JSPS) KAKENHI Grant Number JP17H06300, JP17H06299, JP18H03979.

Animal experiments were performed by Toshiya Kokaji, Atsushi Hatano, and Hiroyuki Kubota. Enzymatic assays, Western blotting measurements, and sample preparation for omics measurements were performed by Atushi hatano and Yuki Ito. Metabolomic analysis using CE-MS was performed by Tomonori Soga and Akiyoshi Hirayama. Lipidomic analysis using LC-MS was performed by Makoto Arita and Kazutaka Ikeda. Transcriptomic analysis using RNA-seq was performed by Yutaka Suzuki. Analysis for sequence data was performed by Yuki Ito. Trans-omic analysis was performed by Toshiya Kokaji.

Finally, I deeply thank my family and friends for their support.

Trans-omic analysis reveals differences in glucose-responsive regulation of
liver metabolism in obese *ob/ob* and wild-type mice

(野生型マウスと *ob/ob* 肥満マウスの肝代謝糖応答性制御のトランスオミクス比較解析)

東京大学大学院新領域創成科学研究科 メディカル情報生命専攻 小鍛治 俊也